Interfaces Free Bound. 28 (2026), 547–594
DOI 10.4171/IFB/547

A minimizing movements approach for crystalline eikonal-curvature flows of spirals

Takeshi Ohtsuka and Yen-Hsi Richard Tsai

Abstract. We propose an algorithm for evolving spiral curves on a planar domain by normal velocities depending on the so-called crystalline curvatures. The algorithm uses a minimizing movements approach and relies on a special level set method for embedding the spirals. We present numerical simulations and comparisons demonstrating the efficacy of the proposed numerical algorithm.

1. Introduction

In this paper, we propose a numerical method for the evolution of spirals in a bounded domain $\Omega \subset \mathbb{R}^2$ by the crystalline curvature flow. We denote the spirals at time t by $\Sigma(t)$, and use $\mathbf{n}$ for a continuous unit normal vector field on $\Sigma(t)$ defining the orientation of the evolution. In this normal direction, the speed of the spirals is formally defined by

$$V_\gamma = -\kappa_\gamma + f, \tag{1.1}$$

where V_γ and κ_γ respectively denote the normal velocity and the crystalline curvature of $\Sigma(t)$ and f is the given driving force. Each spiral in $\Sigma(t)$ is attached to a stationary center denoted by $a_1, \dots, a_N \in \Omega$, and in the evolution of $\Sigma(t)$, portions of different spirals may merge. To describe the merger of spirals during the evolution, we formulate $\Sigma(t)$ by the level set method developed in [28, 31]. In this formulation, $\Sigma(t)$ and $\mathbf{n}$ are given by

$$\Sigma(t) = \{x \in \overline{W} : u(t,x) - \theta(x) \equiv 0 \mod 2\pi\mathbb{Z}\}, \quad \mathbf{n} = -\frac{\nabla(u-\theta)}{|\nabla(u-\theta)|}, \tag{1.2}$$

with an auxiliary function $u(t,x)$ and the predetermined function

$$\theta(x) = \sum_{j=1}^{N} m_j \arg(x - a_j),$$

Mathematics Subject Classification 2020: 35K65 (primary); 53E10, 65M06, 65K10, 53A04 (secondary).
Keywords: crystalline curvature flow, level set method for spirals, total variation minimizing, split Bregman method.

where $\arg(x)$ denotes the argument of $x \in \mathbb{R}^2$ and $m_j \in \mathbb{Z} \setminus \{0\}$, $W = \Omega \setminus (\bigcup_{j=1}^{N} \overline{B_r(a_j)})$, and $B_r(a)$ denotes an open disc with center $a \in \mathbb{R}^2$ and a radius $r > 0$. The domain W is chosen so that the singularity of $\arg(x - a_j)$ is removed from Ω, and thus $\Sigma(t)$ is well defined in (1.2), even though θ is a multi-valued function.

Crystalline mean curvature flow is an anisotropic mean curvature flow with a singular and nonlocal surface energy density. We refer to the survey paper [17] for the crystalline mean curvature flow, and the book [16] for a level set formulation of the geometric evolution equation. A level set formulation of (1.2) yields that

$$V_\gamma = \frac{u_t}{\gamma(\nabla(u - \theta))}, \quad \kappa_\gamma = -\mathrm{div}[\xi(\nabla(u - \theta))],$$

where $\gamma = \gamma(p) \in C^2(\mathbb{R}^2 \setminus \{0\})$ and $\xi = (\partial_{p_1}\gamma, \partial_{p_2}\gamma)$ for $p = (p_1, p_2)$ denotes an anisotropic surface energy density and the Cahn–Hoffman vector, respectively. Hence, (1.1) will be represented as

$$u_t - \gamma(\nabla(u - \theta))\big\{\mathrm{div}[\xi(\nabla(u - \theta))] + f\big\} = 0 \quad \text{in } (0, T) \times W. \tag{1.3}$$

The Wulff diagram associated with γ is defined as

$$\mathcal{W}_\gamma = \big\{p \in \mathbb{R}^2 : \gamma^\circ(p) \le 1\big\} \quad \text{where } \gamma^\circ(p) = \sup\big\{p \cdot q : \gamma(q) \le 1\big\}.$$

An important feature of the crystalline curvature κ_γ is that $\kappa_\gamma \equiv 1$ on the boundary $\partial\mathcal{W}_\gamma$, which is a convex polygon (see [6] for details). It is therefore natural to identify a piecewise linear γ° by $\tilde{n}_j \in \mathbb{R}^2 \setminus \{0\}$ for $j = 0, \ldots, N_\gamma - 1$, using the formula

$$\gamma^\circ(p) = \max_{0 \le j \le N_\gamma - 1} \tilde{n}_j \cdot p.$$

Consequently, γ is also a piecewise linear, that is,

$$\gamma(p) = \max_{0 \le j \le N_\gamma - 1} n_j \cdot p \tag{1.4}$$

for some $n_j \in \mathbb{R}^2 \setminus \{0\}$ for $j = 0, \ldots, N_\gamma - 1$. See [34]. We point out that it is not immediately clear how to make sense of (1.3) classically, as it involves formally taking the first and second derivatives of γ. In this paper, we propose a new numerical algorithm to compute the solution of (1.3), particularly with γ of the form (1.4), in the sense of a weak formulation.

The variational approach by [2, 9] is a powerful option for formulating our problem. Almgren, Taylor, and Wang [2] launched an algorithm for the isotropic mean curvature flow by regarding it as a minimizing problem of the functional that consists of its perimeter and deformation. This idea is also extended to the problem with driving force by [23], or the crystalline case by [1]. Chambolle [9] proposed an algorithm combining the above idea and a level set method using a signed distance function from an interface. This algorithm includes the minimization of the total variation of u, interpreted as minimizing the perimeter of each of u's level sets, and the L^2 norm, which measures the deformation from one discrete step to the next. Therefore, one may consider a splitting algorithm for the minimization problem, using more efficient algorithms for the total variation and L^2 minimization separately and iteratively. Oberman, Osher, Takei, and the second author [26] proposed an algorithm with split Bregman method [18] for interface motion by mean curvature, and extend it to the crystalline case. The goal of this paper is to extend the algorithm by [26] to the evolution of spirals.

We now quickly review the formulation in [9]. Let $\Omega \subset \mathbb{R}^2$ be a domain and $\Sigma \subset \Omega$ be a given interfacial curve, separating Ω into two disjoint subsets. Let $d_\Sigma \colon \Omega \to \mathbb{R}$ be a signed distance function to Σ such that d_Σ is positive inside of Σ. The minimizer w^* of the functional

$$E(w) = \int_\Omega \gamma(\nabla w)dx + \frac{1}{2h}\|w - d_\Sigma\|_{L^2}^2$$

formally satisfies

$$-\mathrm{div}[\xi(\nabla w^*)] + \frac{w^* - d_\Sigma}{h} = 0.$$

Note that $-\mathrm{div}[\xi(\nabla w^*)]$ denotes an anisotropic curvature of level sets of w^* with an anisotropic energy density γ (see [16]). Moreover, Σ moves to the region of $\{x \in \Omega : d_\Sigma(x) < 0\}$ when $V > 0$. Hence, one can find that

$$\Sigma_h := \left\{x \in \Omega : w^*(x) = 0\right\} = \left\{x \in \Omega : d_\Sigma(x) = -h\mathrm{div}[\xi(\nabla w^*(x))]\right\}$$

is the result of the evolution of Σ by $V = -\kappa_\gamma$ in a short time interval $[0, h]$.

When we apply the above idea to our problem, it is natural to consider the minimization problem of the form

$$w \mapsto \int_W \gamma(\nabla(w - \theta))dx - \int_W f w dx + \frac{\|w - g\|_{L^2}^2}{2h}, \tag{1.5}$$

where g is a function relating to the signed "difference" from the current state of spiral $\Sigma(t) \subset \overline{W}$. However, one cannot take g as the "signed distance function" because $\Sigma(t)$ is not an interfacial curve. Indeed, a spiral curve is an open curve in general so that it does not divide the domain into two regions. For this problem, the level set method by [28, 31] overcomes this issue by considering (1.2) instead of the level set of u. Therefore, one option is to construct $g \in C(\overline{W})$ so that $g - \theta \equiv M d_\Sigma$ in a neighborhood of $\Sigma(t)$, where $M \geq 1$ is a constant that is chosen so that g is continuous on $\overline{W}$. (Note that there is a preliminary report [29] in which the first author mentions this algorithm.) Unfortunately, however, it may be necessary to choose an extremely large M, in particular when there is a center having multiple spirals, and the resulting algorithm does not seem particularly robust. To overcome these difficulties, we choose a general level set function, that is, $u_n = u(nh, x)$ to replace g instead of a signed distance function. Then, we consider the minimizing problem of the form

$$w \mapsto \int_W \gamma(\nabla(w - \theta))dx - \int_W f w dx + \frac{1}{2h}\left\|\frac{w - u_n}{\sqrt{\gamma(\nabla(u_n - \theta))}}\right\|_{L^2}^2 \tag{1.6}$$

instead of (1.5). If w^* is the minimizer of the above, then it formally yields the finite difference approximation of (1.3). Thus, we set $u_{n+1} = w^*$ and continue to solve the above with replaced u_n by u_{n+1}.

Our idea leads to two crucial improvements: our algorithm does not require computing the signed distance to a curve, and we may choose $m_j \in \mathbb{Z} \setminus \{0\}$ so that $|m_j|$ is large. In fact, if $|m_j| \gg 1$, then the spiral curves are very crowded around the center a_j. This situation is too difficult to compute by the algorithm using the signed distance without additional adaptivity in meshing. In particular, the second improvement enables us to treat the bunching phenomena. In experimental crystal growth, interlace patterns or so-called illusory spirals and loops are reported in [35, 40]. Our formulation can be applied to such situations.

We briefly mention a special case when u_n in (1.6) has a "flat" portion, that is, the set $\{x \in \overline{W} : \nabla(u_n(x) - \theta(x)) = 0\}$ has an interior, which causes not only the issue of the zero division in (1.6), but also the nonuniqueness of the evolution. Such a case is referred to as "fattening." Evans and Spruck [13] pointed out the possibility of the development of an interior in the level set equation for mean curvature flows. In the set-theoretic approach, Soner [36] gave an example in which fattening occurs. The existing consistency and convergence results for mean curvature flows, such as threshold dynamics by Merriman, Bence, and Osher [24], or the singular limit of the Allen–Cahn equation [5, 10, 12], are established under the smooth evolution or the case when fattening never occurs; see, for example, [4] for the MBO algorithm or [5, 12] for the singular limit of the Allen–Cahn equation. Indeed, these methods may not admit the fattening since they consist of regularization and re-initialization in every iteration. On the other hand, the solution computed by our approach may admit the development of a flat region, which remains stationary until some other portions of the spiral curve approach it. In (1.6), we introduce a cut-off $\max\{\gamma(\nabla(u - \theta)), \alpha\}$ with a small constant $\alpha > 0$ to avoid the zero division. This means that our approach approximates the solution to a level set equation of (1.1) with an approximation regularizing the normal velocity of level sets.

We mention the pioneering front-tracking approach of [3, 37] on crystalline curvature motion. This idea has been also extended to the evolution of a single spiral by [19, 20]. This approach is very convenient to compute crystalline curvature flows of a single spiral in a class of admissible curves. Therefore, we compare our approach and the model due to [20] as a benchmark test. The value of our approach is in its flexibility to be applied in situations where spirals may merge (and thus breaking the admissibility condition for the algorithm of [20]).

In summary, in this paper we deal with spiral curves for which signed distance functions cannot be defined. In Section 2, we propose a new minimizing movements formulation, generalizing Chambolle's formulation to crystalline eikonal-curvature flows of spiral curves. We also present analytical results that provide a theoretical foundation for the proposed algorithm. In Section 3, we offer an efficient numerical algorithm for the proposed minimizing movements formulation. In Section 4, we provide a few numerical simulations and comparisons. Also, in Section 4, we generalize the algorithm to simulate motion laws involving multiple anisotropies. We conclude in Section 5.

2. The proposed formulation

In this section, we propose a minimizing movements formulation for the evolution of spirals by a normal velocity of the form defined in (1.1). The spirals are embedded by the level set method developed in [28, 31].

2.1. The level set method for evolving spirals

We first review the level set method for evolving spirals due to [28, 31] and its evolution equation for an anisotropic eikonal-curvature flow.

Let $\Omega \subset \mathbb{R}^2$ be a bounded domain with smooth boundary. We denote the centers of spirals by $a_1, a_2, \dots, a_N \in \Omega$. We remove small discs $B_r(a_j) = \{x \in \mathbb{R}^2 : |x - a_j| < r\}$ for $j = 1, \dots, N$ from Ω, and set the domain for spiral growth to be

$$W = \Omega \setminus \bigcup_{j=1}^{N} \overline{B_r(a_j)}.$$

We choose $r > 0$ satisfying $\overline{B_r(a_i)} \cap \overline{B_r(a_j)} = \emptyset$ if $i \neq j$, and $\overline{B_r(a_j)} \subset \Omega$ so that ∂W is smooth. Let $m_j \in \mathbb{Z}$ be a signed number of spirals associated with a_j, meaning

- $|m_j|$ curves are attached to a_j as their endpoint,
- if $m_j > 0$ (resp. $m_j < 0$), then these curves rotate around a_j with counterclockwise (resp. clockwise) rotation when $V_\gamma > 0$.

Our level set representation of spirals relies on a predetermined function θ that is first introduced for a phase-field model of evolving spirals [22, 25]. Define

$$\theta(x) = \sum_{j=1}^{N} m_j \arg(x - a_j).$$

Let $\Sigma(t) \subset \overline{W}$ be the evolving spirals at time $t \geq 0$, and $\mathbf{n} \in \mathbb{S}^1$ be a continuous unit normal vector field of $\Sigma(t)$ denoting the orientation of the evolution of $\Sigma(t)$. Then, we describe $\Sigma(t)$ and $\mathbf{n}$ by

$$\Sigma(t) = \left\{x \in \overline{W} : u(t,x) - \theta(x) \equiv 0 \mod 2\pi\mathbb{Z}\right\}, \quad \mathbf{n} = -\frac{\nabla(u - \theta)}{|\nabla(u - \theta)|} \tag{2.1}$$

with an auxiliary function $u\colon [0, T) \times \overline{W} \to \mathbb{R}$ for some $T > 0$. Note that θ should be a multi-valued function to describe the spirals. However, $\nabla\theta$ can be defined as a single-valued function.

Let $\gamma\colon \mathbb{R}^2 \to [0,\infty)$ be convex, continuous, positively homogeneous of degree 1, and positive on $\mathbb{S}^1$. It defines an anisotropic surface energy density. According to [16], an anisotropic curvature κ_γ of $\Sigma(t)$ with (2.1) is of the form

$$\kappa_\gamma = -\mathrm{div}[\xi(\nabla(u-\theta))] \tag{2.2}$$

provided that $\gamma \in C^2(\mathbb{R}^2 \setminus \{0\})$, where $\xi(p) = (\partial_{p_1}\gamma, \partial_{p_2}\gamma)$ for $p = (p_1, p_2)$. In fact, $\gamma(p) = |p|$ reduces the above to the isotropic curvature. Note that (2.2) can be interpreted as the first variation of the anisotropic energy

$$\int_W \gamma(\nabla(u-\theta))dx$$

for the level sets of $u - \theta$. This viewpoint will be convenient to understand the algorithms of [2, 9].

The support function of $\{p \in \mathbb{R}^2 : \gamma(p) \le 1\}$, denoted by

$$\gamma^\circ(p) = \sup\{p\cdot q : \gamma(q) \le 1\},$$

plays important roles for the anisotropic curvature flow. In fact, the following hold:

- If $\gamma, \gamma^\circ \in C^2(\mathbb{R}^2 \setminus \{0\})$, then for $p \in \mathbb{R}^2 \setminus \{0\}$ we have

$$\gamma(\nabla\gamma^\circ(p)) = \gamma^\circ(\nabla\gamma(p)) = 1, \tag{2.3}$$

$$\nabla\gamma(\nabla\gamma^\circ(p)) = \frac{p}{\gamma^\circ(p)}, \tag{2.4}$$

$$\nabla\gamma^\circ(\nabla\gamma(p)) = \frac{p}{\gamma(p)}.$$

.

- $\gamma^{\circ\circ}(p) = \gamma(p)$.

See [6] and [34] for details.

Equation (2.4) yields that

$$\kappa_\gamma = 1 \quad \text{on } \partial\mathcal{W}_\gamma, \text{ where } \quad \mathcal{W}_\gamma = \{p \in \mathbb{R}^2 : \gamma^\circ(p) \le 1\}.$$

In other words, by the analogy from the isotropic curvature, the Wulff diagram plays the role of a unit ball in the anisotropic curvature flow. Thus, we introduce the Finsler metric

$$d_\gamma(x, y) = \gamma^\circ(x - y). \tag{2.5}$$

(Note that this metric is possibly not symmetric, since we do not assume γ is symmetric.) Then, (2.3) implies $\gamma(\nabla d_\gamma(\cdot, y)) = 1$ in $\{x : d_\gamma(x, y) > 0\}$. This is a generalized result of $|\nabla d| = 1$ for isotropic distance $d(x, y) = |x - y|$. Following this fact, we introduce an anisotropic normal velocity V_γ for $\Sigma(t)$, which is of the form

$$V_\gamma = \frac{u_t}{\gamma(\nabla(u-\theta))}.$$

This is analogous to the isotropic normal velocity $V = u_t/|\nabla u|$ for the level set $\{x : u(t,x) = 0\}$. Consequently, we obtain the level set equation of (1.1) as follows:

$$u_t - \gamma(\nabla(u-\theta))\big\{\mathrm{div}[\xi(\nabla(u-\theta))] + f\big\} = 0 \quad \text{in } (0,T)\times W. \tag{2.6}$$

This paper primarily concerns the crystalline curvature flow, that is, the cases in which $\mathcal{W}_\gamma$ is a convex polygon with N_γ sides ($N_\gamma \geq 3$). For these cases, it is natural to write γ° as

$$\gamma^\circ(p) = \max_{0\leq j\leq N_\gamma-1} \widetilde{n}_j \cdot p \quad \text{with} \quad \widetilde{n}_j = \widetilde{r}_j(\cos\widetilde{\vartheta}_j, \sin\widetilde{\vartheta}_j) \in \mathbb{R}^2 \setminus \{0\}.$$

Here we assume that $\{\widetilde{n}_j : j = 0, \ldots, N_\gamma - 1\}$ satisfies the following, so that $\mathcal{W}_\gamma$ is a convex polygon:

(W1) $\widetilde{\vartheta}_j \in [\widetilde{\vartheta}_0, \widetilde{\vartheta}_0 + 2\pi]$ for $j = 0, 1, 2, \ldots, N_\gamma - 1$.

(W2) $\widetilde{\vartheta}_j < \widetilde{\vartheta}_{j+1} < \widetilde{\vartheta}_j + \pi$ for $j = 0, 1, \ldots, N_\gamma - 1$, where $\widetilde{\vartheta}_{N_\gamma} = \widetilde{\vartheta}_0 + 2\pi$.

(W3) The set $\{\widetilde{n}_j : j = 0, 1, 2, \ldots, N_\gamma - 1\}$ is minimal, that is,

$$\gamma^\circ(p) \neq \max\{\widetilde{n}_j \cdot p : j \neq k\}$$

for any $k \in \{0, \ldots, N_\gamma - 1\}$.

By $\gamma^{\circ\circ} = \gamma$ and conditions (W1)–(W3), there exist $\vartheta_j \in \mathbb{R}$ for $j = 0, \ldots, N_\gamma - 1$ which satisfy

$$\gamma(p) = \max_{0\leq j\leq N_\gamma-1} n_j \cdot p \quad \text{with} \quad n_j = r_j(\cos\vartheta_j, \sin\vartheta_j) \in \mathbb{R}^2 \setminus \{0\}. \tag{2.7}$$

Moreover, $\{n_j : j = 0, \ldots, N_\gamma - 1\}$ still satisfies (W1)–(W3). The typical example of γ and γ° is

$$\gamma(p) = \|p\|_{\ell^1}, \quad \gamma^\circ(p) = \|p\|_{\ell^\infty},$$

and thus $\mathcal{W}_\gamma = [-1, 1]^2$. It is given by

$$n_j = \sqrt{2}\Big(\cos\frac{\pi(2j+1)}{4}, \sin\frac{\pi(2j+1)}{4}\Big), \quad \widetilde{n}_j = \Big(\cos\frac{\pi j}{2}, \sin\frac{\pi j}{2}\Big).$$

In general, the following are required of γ for the crystalline curvature flow:

(A1) $\gamma : \mathbb{R}^2 \to [0, \infty)$ is convex.

(A2) γ is positively homogeneous of degree 1.

(A3) There exists $\Lambda_\gamma > 0$ such that $\Lambda_\gamma^{-1} \leq \gamma \leq \Lambda_\gamma$ on $\mathbb{S}^1$.

(A4) $\mathcal{W}_\gamma = \{p : \gamma^\circ(p) \leq 1\}$ is a convex polygon.

Note that any γ given by (2.7) with (W1)–(W3) satisfies (A1)–(A4).

2.2. The proposed minimizing movements

Now, let the spiral $\Sigma \subset \overline{W}$ be given as

$$\Sigma = \left\{x \in \overline{W} : u(x) - \theta(x) \equiv 0 \mod 2\pi\mathbb{Z}\right\}$$

with $u \in C(\overline{W})$. Corresponding to the level set equation defined in (2.6), we consider minimizing the energy functional

$$w \mapsto \int_W \gamma(\nabla(w-\theta))dx - \int_W f w dx + \frac{1}{2h}\left\| \frac{w-u}{\sqrt{\gamma(\nabla(u-\theta))}} \right\|_{L^2}^2. \tag{2.8}$$

Formally, the minimizer w^* satisfies

$$-\mathrm{div}[\xi(\nabla(w^* - \theta))] - f + \frac{w^* - u}{h\gamma(\nabla(u-\theta))} = 0,$$

which implies

$$w^* = u + h\gamma(\nabla(u-\theta))\left\{\mathrm{div}[\xi(\nabla(w^*-\theta))] + f\right\}. \tag{2.9}$$

On the other hand, the implicit Euler scheme of (2.6) takes the form

$$u(t+h) = u(t) + h\gamma(\nabla(u(t+h)-\theta))\left\{\mathrm{div}[\xi(\nabla(u(t+h)-\theta))] + f\right\}. \tag{2.10}$$

Comparing (2.9) and (2.10), we define

$$S_h(\Sigma) = \left\{x \in \overline{W} : w^*(x) - \theta(x) \equiv 0 \mod 2\pi\mathbb{Z}\right\}$$

as the result of the evolution of Σ for a short time step $h > 0$. We can now iterate the stepping as follows:

(1) For given Σ_n ($n \geq 0$) and $u_n \in C(\overline{W})$ satisfying

$$\Sigma_n = \left\{x \in \overline{W} : u_n(x) - \theta(x) \equiv 0 \mod 2\pi\mathbb{Z}\right\},$$

compute the minimizer w^* of (2.8) with $u = u_n$.

(2) Set $u_{n+1} = w^*$ and

$$\Sigma_{n+1} = \left\{x \in \overline{W} : u_{n+1}(x) - \theta(x) \equiv 0 \mod 2\pi\mathbb{Z}\right\}.$$

This algorithm can be applied even if γ is not smooth, and we can then define $\Sigma(t) = \Sigma_n$ when $nh \leq t < (n+1)h$.

Remark 2.1. Formally, if $u - \theta$ is a signed distance by (2.5), then (2.8) is reduced to (1.5) by (2.3). In other words, the first variation of the term $\|w - d_\Sigma\|_{L^2}^2$ in Chambolle's algorithm or $\|(w-u)/\sqrt{\gamma(\nabla(u-\theta))}\|_{L^2}^2$ in (2.8) approximates the normal velocity of the evolving level set, where d_Σ denotes the distance function from Σ.

From another viewpoint, for Chambolle's algorithm, one has to choose the function u satisfying $\gamma(\nabla(u-\theta)) = 1$ at least in a tubular neighborhood of Σ. This is the reason why Chambolle's algorithm requires the process of constructing the distance function.

Remark 2.2. The proposed algorithm is not justified when $\{x \in \overline{W} : \nabla(u_n - \theta)(x) = 0\}$ has a nonempty interior. This means that the integrand of the functional in (2.8) will formally involve a division by zero. Unfortunately, when we consider the evolution of interfacial curve (i.e., $\theta \equiv 0$), there exists an example such that a level set $\{x \in \Omega : u(t,x) = c\}$ has a nonempty interior for $t > 0$, even though $\{x \in \Omega : u(0,x) = c\}$ does not have an interior. Let us consider the following isotropic eikonal-curvature motion:

$$u_t - |\nabla u|\Big\{\mathrm{div}\Big(\frac{\nabla u}{|\nabla u|}\Big)+1\Big\} = 0 \quad \text{in } (0,T)\times\Omega,$$
$$u(0,x) = -|x_2| \quad \text{for } x = (x_1,x_2) \in \Omega$$

with $\Omega = (\mathbb{R}/(2\mathbb{Z}))^2$. Then, one can find that

$$u(t,x) = \min\big\{0, t - |x_2|\big\}$$

is a viscosity solution to the above problem. However, $\{x \in \Omega : u(t,x) = 0\}$ has nonempty interior for every $t > 0$.

In the practical stage, when fattening develops, we will introduce a cut-off of $\gamma(\nabla(u-\theta))$ to avoid division by zero; see Sections 2.3 and 3.3.

Remark 2.3. When we consider (1.1) with a more general mobility term of the form

$$\beta(-\mathbf{n})V_\gamma = -\kappa_\gamma + f, \quad \beta \neq 0,$$

one can set u_{n+1} as

$$u_{n+1} = u_n + \frac{w^* - u_n}{\beta(\nabla(w^* - \theta))},$$

where w^* is the minimizer of (2.8).

2.3. Existence of minimizing movements

In this subsection, we prove the existence of the sequence $\{u_n\}$ satisfying our proposed algorithms. We shall address two essential questions on (i) the existence of a minimizer of (2.8) for u_n, and (ii) whether the obtained minimizer u_{n+1} has ∇u_{n+1} again.

We first give a rigorous definition of the functional $w \mapsto \int_W \gamma(\nabla(w-\theta))dx$ to find the minimizer of E. By analogy of the total variation

$$[u]_{BV} := \sup\Big\{-\int_W u \,\mathrm{div}\varphi dx : \varphi \in C_c^1(W;\mathbb{R}^2),\ |\varphi| \leq 1\Big\}$$

and $\gamma(p) = (\gamma^\circ)^\circ(p) = \sup\{p\cdot q : \gamma^\circ(q) \leq 1\}$ when γ is convex, let us define $J_\gamma\colon L^1(W) \to [0,\infty]$ by

$$J_\gamma(w) = \sup\Big\{-\int_W w \,\mathrm{div}\varphi dx - \int_W \nabla\theta\cdot\varphi dx : \varphi \in C_c^1(W;\mathbb{R}^2),\ \gamma^\circ(\varphi) \leq 1\Big\}. \quad (2.11)$$

We obtain the following fundamental properties by a standard argument:

Lemma 2.4. *Assume that* (A1)–(A3) *hold. Then, the following hold:*

(1) J_γ *is convex, and* $J_\gamma \geq 0$.

(2) *If* $w \in BV(W)$, *then* $J_\gamma(w) < \infty$.

(3) $\liminf_{u \to v} J_\gamma(u) \geq J_\gamma(v)$ *in* $L^1(W)$.

(4) *If* $w \in W^{1,1}(W)$, *then* $J_\gamma(w) = \int_W \gamma(\nabla(w - \theta))dx$.

See Appendix B for the proof of Lemma 2.4.

According to the result of Lemma 2.4, we now define $E(\cdot; g) \colon L^2(W) \to \mathbb{R} \cup \{\infty\}$. For given $f, g \in L^2(W)$ and $\psi \colon W \to \mathbb{R}$ such that $\varphi/\sqrt{\psi} \in L^2(W)$ for every $\varphi \in L^2(W)$, define

$$E(w; g) := \begin{cases} J_\gamma(w) - \displaystyle\int_W f w dx + \frac{1}{2h}\left\| \frac{w - g}{\sqrt{\psi}} \right\|_{L^2}^2 & \text{if } w \in L^2(W) \cap BV(W), \\ \infty & \text{otherwise.} \end{cases} \tag{2.12}$$

Lemma 2.5. *Assume that* (A1)–(A3) *hold, and there exist positive constants* α, A *satisfying*

$$0 < \alpha < \psi < A \quad \text{on } W. \tag{2.13}$$

Let $w \in L^2(W) \cap BV(W)$ *be such that* $E(w; g) \leq R$ *for some constant* $R > 0$. *Then, there exist positive constants* C_0 *and* C_1 *such that*

$$\|w\|_{BV} + \|w\|_{L^2} \leq C_0 + C_1 \eta^2 \tag{2.14}$$

for $\eta = \sqrt{hA}$, *where* $\|w\|_{BV} = \|w\|_{L^1} + [w]_{BV}$.

Proof. Note that C_0, C_1, and C_2 in the following discussions denote numerical constants, which will be changed by calculations.

We first demonstrate that

$$\max\{\|w\|_{L^1}, \|w\|_{L^2}\} \leq C_0 + C_1\eta + C_2\eta^2. \tag{2.15}$$

By straightforward calculation, we have

$$\begin{aligned} E(w; g) &\geq J_\gamma(w) + \frac{1}{2hA}\int_W [(w - g)^2 - 2hAfw]dx \\ &= J_\gamma(w) + \frac{1}{2hA}\int_W [(w - (g + hAf))^2 - (g + hAf)^2 + g^2]dx \\ &\geq J_\gamma(w) + \frac{1}{2hA}(\|w - G\|_{L^2}^2 - \|G\|_{L^2}^2), \end{aligned} \tag{2.16}$$

where $G = g + hAf$. Then, we first obtain

$$\|w - G\|_{L^2} \leq \sqrt{2hAR + \|G\|_{L^2}^2} \leq \sqrt{2hAR} + \|G\|_{L^2}$$

by $E(w; g) \leq R$ and $J_\gamma(w) \geq 0$. Hence, we obtain

$$\|w\|_{L^2} \leq \sqrt{2hAR} + 2\|G\|_{L^2} \leq \sqrt{2hAR} + 2(\|g\|_{L^2} + hA\|f\|_{L^2}) = C_0 + C_1\eta + C_2\eta^2.$$

This also implies that

$$\|w\|_{L^1} \leq |W|\|w\|_{L^2} \leq C_0 + C_1\eta + C_2\eta^2,$$

since W is bounded. Hence, we obtain (2.15).

For the bound of $[w]_{BV}$, one can find

$$J_\gamma(w) - \int_W f w dx \leq E(w; g) \leq R.$$

Let $\varphi \in C_c^1(W; \mathbb{R}^2)$ be such that $|\varphi| \leq 1$. Then, since $\widetilde{\varphi} = \Lambda_\gamma^{-1}\varphi$ satisfies $\gamma^\circ(\widetilde{\varphi}) \leq 1$, we obtain

$$\begin{aligned}
-\int_W w \operatorname{div}\varphi dx &= \Lambda_\gamma\Big(-\int_W w \operatorname{div}\widetilde{\varphi} dx\Big) \leq \Lambda_\gamma\Big(J_\gamma(w) + \int_W \nabla\theta \cdot \widetilde{\varphi} dx\Big) \\
&\leq \Lambda_\gamma\Big(R + \int_W f w dx\Big) + \int_W \nabla\theta \cdot \varphi dx \\
&\leq \Lambda_\gamma R + |W|\|\nabla\theta\|_\infty + \Lambda_\gamma\|f\|_{L^2}\|w\|_{L^2}.
\end{aligned}$$

It implies

$$[w]_{BV} = C_0 + C_1\eta + C_2\eta^2,$$

and thus $\|w\|_{BV} \leq C_0 + C_1\eta + C_2\eta^2$. Since $\eta \leq (1 + \eta^2)/2$, we obtain (2.14). ∎

Theorem 2.6. *Assume that (A1)–(A3) hold. Then, for every $f, g \in L^2(W)$ and $\psi: W \to \mathbb{R}$ satisfying (2.13), there exists a unique minimizer $w^* \in L^2(W) \cap BV(W)$ of $E(w; g)$.*

Proof. By (2.16), we observe that

$$-\infty < -\|G\|_{L^2}^2/(2hA) \leq \inf_{L^2(W)\cap BV(W)} E(\cdot; g) \leq E(0; g) < \infty.$$

Thus, there exists $w_n \in L^2(W) \cap BV(W)$ such that

$$\lim_{n\to\infty} E(w_n; g) = \inf_{w \in L^2(W)\cap BV(W)} E(w; g).$$

We observe that $E(w_n; g) \leq E(0; g) + 1$ for sufficiently large n, and thus the sequence $\{w_n\}$ is bounded in $L^2(W) \cap BV(W)$ by Lemma 2.5. This implies that there exists a subsequence of $w_n \in L^2(W) \cap BV(W)$, which is still denoted by w_n, and $w^* \in L^2(W) \cap BV(W)$ such that $w_n \rightharpoonup w^*$ in $L^2(W)$ and $\|w_n - w^*\|_{L^1} \to 0$ as $n \to \infty$;

see [11, §5.2.3]. It implies

$$E(w^*; g) \le \liminf_{n\to\infty} E(w_n; g) = \inf_{w\in L^2(W)\cap BV(W)} E(w; g),$$

since $E(\cdot; g)$ is lower semicontinuous in $L^1(W)$ by Lemma 2.4(3). Hence, w^* is the minimizer of E.

Uniqueness is derived from the strict convexity of $E(\cdot; g)$ on $L^2(W)\cap BV(W)$, which is obtained since $\|(w-g)/\sqrt{\psi}\|_{L^2}^2$ is strictly convex for $w \in L^2(W)\cap BV(W)$. ■

We next discuss the second problem, that is, the minimizer $w^* \in L^2(W)\cap BV(W)$ of E has a function ∇w^* on W. Now, let $w \in BV(W)$. According to the theory of functions of bounded variation, there exists a Radon measure ν and a ν-measurable function $\sigma : W \to \mathbb{R}^2$ satisfying

- $|\sigma| = 1$ ν-almost everywhere in W,
- $\int_W w \operatorname{div}\varphi dx = -\int_W \varphi\cdot\sigma d\nu$ for every $\varphi \in C_c^1(W;\mathbb{R}^2)$.

See [11, §5]. Let $\sigma = (\sigma^1, \sigma^2)$ and define the signed measures

$$\nu^i(U) = \int_U \sigma^i d\nu \quad (i = 1, 2)$$

for every Borel set $U \subset W$. Then, Lebesgue's decomposition theorem implies that there exist signed measures ν_{ac}^i and ν_{s}^i such that

- $\nu^i = \nu_{\mathrm{ac}}^i + \nu_{\mathrm{s}}^i$ for $i = 1, 2$. This decomposition is unique for $i = 1, 2$.
- ν_{ac}^i is absolutely continuous, and ν_{s}^i is singular for the Lebesgue measure $\mathcal{L}^2$ in $\mathbb{R}^2$.
- There exists a function $u^i \in L^1(W)$ such that

  $$\nu_{\mathrm{ac}}^i(U) = \int_U u^i dx \quad (i = 1, 2)$$

  for every Borel set $U \subset W$.

By combining the above, we observe that

$$\int_W w \operatorname{div}\varphi dx = -\sum_{i=1}^2 \Big(\int_W \varphi^i d\nu_{\mathrm{ac}}^i + \int_W \varphi^i d\nu_{\mathrm{s}}^i\Big) = -\sum_{i=1}^2 \int_W u^i \varphi^i dx + \Phi_{\mathrm{s}}(\varphi) \quad (2.17)$$

for every $\varphi = (\varphi^1, \varphi^2) \in C_c^1(W;\mathbb{R}^2)$, where $\Phi_{\mathrm{s}}(\varphi) := -\sum_{i=1}^2 \int_W \varphi^i d\nu_{\mathrm{s}}^i$. From (2.17), notice that $w \in W_{\mathrm{loc}}^{1,1}(W)$ if and only if $w \in L_{\mathrm{loc}}^1(W)$, $(u^1, u^2) \in L_{\mathrm{loc}}^1(W)$, and $\Phi_s \equiv 0$. Hence, we define the weak derivative of $w \in BV(W)$ by

$$\nabla w := (u^1, u^2). \quad (2.18)$$

Now, let $u_n \in L^2(W)\cap BV(W)$ be given for our algorithm. For positive constants $\alpha \ll 1$ and $A > \alpha$, set

$$\psi = \psi_n := \min\{\max\{\gamma(\nabla u_n - \nabla\theta), \alpha\}, A\}$$

for $E(\cdot, u_n)$. Then, the minimizer u_{n+1} of $E(\cdot; u_n)$ exists, and also has weak derivative ∇u_{n+1} in the sense of (2.18). Thus, we can continue the time-stepping iterations of our algorithm. Consequently, we conclude this section by presenting the following result for our proposed algorithms:

Theorem 2.7. *Let $f \in L^2(W)$, $u_0 \in L^2(W) \cap BV(W)$. Let $h > 0$, and $0 < \alpha < A < \infty$ be constants. Then, there exists a unique sequence $\{u_n\}_{n\geq 0} \subset L^2(W) \cap BV(W)$ such that*

$$\begin{aligned} u_{n+1} &= \arg \min_{L^2(W)\cap BV(W)} E(\cdot; u_n) \\ &\textit{with} \quad \psi = \min\big\{\max\big\{\gamma(\nabla u_n - \nabla\theta), \alpha\big\}, A\big\}, \end{aligned}$$

where ∇u_n is in the sense of (2.18).

3. Numerics for the proposed minimizing movements

This section describes how we use the split Bregman method to efficiently construct the minimizer of $E(w; g)$ defined in (2.12). We will see that the Split Bregman algorithm, combined with a special shrinkage formula, yields a simple algorithm for crystalline curvature motion. The procedure is then summarized as Algorithm 1.

3.1. The Split Bregman Method

We now review the split Bregman method due to [26] for the calculation of the minimizer w^* of $E(w; g)$.

The key idea to find w^* is to interpret the problem as a constraint minimization problem by dividing the dependent variable: find a minimizer (w^*, d^*) of

$$\begin{aligned} F(w, d) &:= \int_W \gamma(d - \nabla\theta)dx - \int_W fwdx + \frac{1}{2h}\left\|\frac{w-g}{\sqrt{\psi}}\right\|_{L^2}^2 \\ &\text{subject to } d = \nabla w. \end{aligned}$$

To solve this problem, we apply the Bregman iteration due to [7, 33]. Let us introduce the Bregman distance $D_F^{p,q}$ of the form

$$D_F^{p^*,q^*}(w, d; \widehat{w}, \widehat{d}) = F(w, d) - F(\widehat{w}, \widehat{d}) - \langle p^*, w - \widehat{w}\rangle - \langle q^*, d - \widehat{d}\rangle$$

for $p^* \in \partial_w F(\widehat{w}, \widehat{d})$ and $q^* \in \partial_d F(\widehat{w}, \widehat{d})$, where

$$\begin{aligned} \partial_w F(\widehat{w}, \widehat{d}) &= \big\{p \in H^1(W)^* : F(w, \widehat{d}) \geq F(\widehat{w}, \widehat{d}) - \langle p, w - \widehat{w}\rangle \text{ for } w \in H^1(W)\big\}, \\ \partial_d F(\widehat{w}, \widehat{d}) &= \big\{q \in L^2(W; \mathbb{R}^2)^* : F(\widehat{w}, d) \geq F(\widehat{w}, \widehat{d}) - \langle q, d - \widehat{d}\rangle \\ &\qquad\qquad\qquad\qquad\qquad\qquad\qquad \text{for } d \in L^2(W; \mathbb{R}^2)\big\}. \end{aligned}$$

Then, we set

$$(w^{k+1}, d^{k+1}) = \arg \min_{(w,d)\in H^1(W)\times L^2(W;\mathbb{R}^2)} \Big[D_F^{p^k,q^k}(w, d; w^k, d^k) + \frac{\mu}{2}\|d - \nabla w\|_{L^2}^2 \Big],$$
$$(w^0, d^0) = (g, 0), \quad p^k \in \partial_w F(w^k, d^k),\ q^k \in \partial_d F(w^k, d^k).$$

It should hold that $(w^*, d^*) = \lim_{k\to\infty}(w^k, d^k)$.

Next, we rephrase the above iteration. Since $(w, d) \mapsto d - \nabla w$ is linear, the above iteration is equivalent to the following iteration:

$$(w^{k+1}, d^{k+1}) = \arg \min_{(w,d)\in H^1(W)\times L^2(W;\mathbb{R}^2)} \Big[F(w, d) + \frac{\mu}{2}\|d - \nabla w - b^k\|_{L^2}^2 \Big], \tag{3.1}$$
$$b^{k+1} = b^k + \nabla w^{k+1} - d^{k+1}, \tag{3.2}$$
$$(w^0, d^0, b^0) = (g, 0, 0). \tag{3.3}$$

We solve (3.1)–(3.3) by the following alternate iteration:

$$w_{\ell+1}^k = \arg \min_{w\in H^1(W)} \Big[F(w, d_\ell^k) + \frac{\mu}{2}\|d_\ell^k - \nabla w - b^k\|_{L^2}^2 \Big], \tag{3.4}$$
$$d_{\ell+1}^k = \arg \min_{d\in L^2(W;\mathbb{R}^2)} \Big[F(w_{\ell+1}^k, d) + \frac{\mu}{2}\|d - \nabla w_{\ell+1}^k - b^k\|_{L^2}^2 \Big], \tag{3.5}$$
$$(w_0^k, d_0^k) = (w^k, d^k). \tag{3.6}$$

For problem (3.4), we consider the Euler–Lagrange equation of the functional

$$w \mapsto -\int_W f w dx + \frac{1}{2h}\left\| \frac{w - g}{\sqrt{\psi}} \right\|_{L^2}^2 + \frac{\mu}{2}\|d_\ell^k - \nabla w - b^k\|_{L^2}^2,$$

and then solve the following elliptic equation with the below boundary condition:

$$w - h\mu\psi\Delta w = g + h\psi(f - \mu \operatorname{div}(d_\ell^k - b^k)) \quad \text{in } W, \tag{3.7}$$
$$(d_\ell^k - \nabla w - b^k)\cdot \vec{\nu} = 0 \quad \text{on } \partial W, \tag{3.8}$$

where $\vec{\nu}$ denotes the outer unit normal vector field of W. The problem defined in (3.5) is to find the minimizer of

$$d \mapsto \int_W \gamma(d - \nabla\theta) dx + \frac{\mu}{2}\|d - \nabla w_{\ell+1}^k - b^k\|_{L^2}^2.$$

It is solved by considering the minimizer of the integrand, i.e.,

$$d_{\ell+1}^k(x) = \arg \min_{d\in\mathbb{R}^2} \Big[\gamma(d - \nabla\theta(x)) + \frac{\mu}{2}|d - \nabla w_{\ell+1}^k(x) - b^k(x)|^2 \Big] \tag{3.9}$$

for every $x \in \overline{W}$. It is mentioned in the next subsection.

Remark 3.1. Note that we shall use $\psi = \gamma(\nabla(g - \theta))$ directly for (3.7) as we will mention in Section 3.4. In this case, one finds that (3.7) is degenerate in an interior of the set where $\nabla(g - \theta) = 0$. However, numerically it means $w^* = g$ there. It seems to be consistent with the minimizing movement because of the last term of $E(w; g)$.

3.2. Shrinkage function

We calculate the polyhedral shrinkage function for the second minimizing problem (3.9) by following [26]. By considering $\tilde{\gamma}(p) = (1/\mu)\gamma(p)$ instead of $\gamma(p)$ if necessary, (3.9) is summarized as follows: find a minimizer x^* of

$$x \mapsto \gamma(x - z) + \frac{1}{2}|x - y|^2 \tag{3.10}$$

for given $y, z \in \mathbb{R}^2$.

First, we consider the necessary condition for the minimizer $x^* = x^*(y, z)$ of (3.10) without assumption (A4). Remark that $\gamma(x)$ is represented as

$$\gamma(x) = \sup_{p \in \mathcal{W}_\gamma} p \cdot x$$

when γ is convex, where $\mathcal{W}_\gamma = \{p \in \mathbb{R}^2 : \gamma^\circ(p) \le 1\}$, and $\gamma^\circ(p) = \sup\{p \cdot q : \gamma(q) \le 1\}$. The following results are a revised version of the formula of x^* and its corollary due to [26]. Since the proofs are similar to those, we omit them. See also [30].

Lemma 3.2. *Let $x^* = x^*(y, z)$ be the minimizer of* (3.10). *Then,*

$$x^* = y - P_{\mathcal{W}_\gamma}(y - z),$$

where $P_{\mathcal{W}_\gamma} : \mathbb{R}^2 \to \mathcal{W}_\gamma$ is the projection map of x onto $\mathcal{W}_\gamma$, which is

$$P_{\mathcal{W}_\gamma}(x) = \arg\min_{y \in \mathcal{W}_\gamma} |y - x|^2.$$

Corollary 3.3. *It holds that $y - z \in \mathcal{W}_\gamma$ if and only if $x^*(y, z) = z$.*

Let us consider the remaining case when $y - z \notin \mathcal{W}_\gamma$. From here on, let γ be a convex and piecewise linear function, that is,

$$\gamma(p) = \max_{0 \le j \le N_\gamma - 1} n_j \cdot p,$$

where $n_j = r_j(\cos\vartheta_j, \sin\vartheta_j)$ ($r_j > 0$ is a constant). We here assume that (W1)–(W3) hold for $\{n_j : j = 0, \dots, N_\gamma - 1\}$. Note that, when (W1) and (W2) hold, (W3) is equivalent to the following property:

(W3)’ $Q_i = \{p \ne 0 : n_i \cdot p > n_j \cdot p \quad \text{for } j \ne i\} \ne \emptyset$, and $Q_i = R_{i,i-1} \cap R_{i,i+1}$, where $R_{j,k} = \{p \ne 0 : n_j \cdot p > n_k \cdot p\}$, and $R_{N_\gamma-1,N_\gamma} := R_{N_\gamma-1,0}$.

Note that (W3)’ implies $\partial Q_i = \Xi_{i-1,i} \cup \Xi_{i,i+1} \cup \{0\}$, where $\Xi_{i,i+1} = \{p \ne 0 : n_i \cdot p = n_{i+1} \cdot p > 0\}$. Moreover, γ is smooth on Q_i and has singularities on each $\Xi_{i,i+1}$. By using the above notations, we now characterize x^* when $y - z \notin \mathcal{W}_\gamma$.

Lemma 3.4. *Let $\gamma(p) = \max_{0 \le j \le N_\gamma - 1} n_j \cdot p$ with $n_j = r_j(\cos\vartheta_j, \sin\vartheta_j)$ for $r_j > 0$ and $\vartheta_j \in \mathbb{R}$, and assume that (W1)–(W3) hold. Let $y, z \in \mathbb{R}^2$ satisfy $y - z \notin \mathcal{W}_\gamma$. Set*

$$\lambda_i = \frac{(y-z)\cdot(n_i - n_{i+1}) - n_i \cdot n_{i+1} + |n_{i+1}|^2}{|n_i - n_{i+1}|^2},$$
$$\xi_i = \lambda_i n_i + (1-\lambda_i) n_{i+1}.$$

Let x^* be the minimizer of (3.10). Then, the following hold:

(1) *If $x^* - z \in \Xi_{i,i+1}$, then*

$$\lambda_i \in [0,1] \quad \text{and} \quad (y - z - \xi_i)\cdot \xi_i \ge 0. \tag{3.11}$$

Moreover, $x^* = y - \xi_i$.

(2) *If $x^* - z \in Q_i$, then*

$$\lambda_i > 1 \quad \text{and} \quad \lambda_{i-1} < 0. \tag{3.12}$$

Moreover, $x^* = y - n_i$.

According to Corollary 3.3 and Lemma 3.4, we introduce the following procedure to obtain d^k_{j+1}:

Scheme (Sh) to obtain $d^k_{\ell+1}$ of (3.5).

We do the following for every $x \in \overline{W}$: set $y = \nabla w^k_{\ell+1}(x) + b^k(x)$ and $z = \nabla\theta(x)$.

Step 1. Check either $y - z \in \mathcal{W}_\gamma$ (i.e., $\gamma^\circ(y-z) \le 1$) or not.

If $y - z \in \mathcal{W}_\gamma$, then $x^* = z$ by Corollary 3.3. Otherwise, we go to the next step.

Step 2. When $y - z \notin \mathcal{W}_\gamma$, check either $x^* - z \in \bigcup_{i=0}^{N_\gamma-1} \Xi_{i,i+1}$ or $x^* - z \in \bigcup_{i=0}^{N_\gamma-1} Q_i$.

Note that Lemma 3.4 gives a necessary condition for the minimizer x^*. Then, we can divide the situation into the two cases below.

Case A. There is no $i \in \{0, 1, 2, \dots, N_\gamma - 1\}$ satisfying (3.11).

In this case we find $x^* - z \notin \bigcup_{i=0}^{N_\gamma-1} \Xi_{i,i+1}$ and then $x^* - z \in \bigcup_{i=0}^{N_\gamma-1} Q_i$. Therefore, find $i_0 \in \{0, 1, \dots, N_\gamma - 1\}$ satisfying (3.12). If there exists such an i_0 uniquely, then set

$$x^* = y - n_{i_0}.$$

If there exist several i satisfying (3.12), choose i_0 that minimizes

$$i \mapsto \gamma(\tilde{x}^*_i - z) + \frac{1}{2}|\tilde{x}^*_i - y|^2 \quad \text{subject to (3.12)},$$

where $\tilde{x}^*_i = y - n_i$.

Case B. There is no $i \in \{0, 1, 2, \ldots, N_\gamma - 1\}$ **satisfying** (3.12)**.**

In this case we find $x^* - z \notin \bigcup_{i=0}^{N_\gamma - 1} Q_i$ and then $x^* - z \in \bigcup_{i=0}^{N_\gamma - 1} \Xi_{i,i+1}$. Therefore, find $i_0 \in \{0, 1, \ldots, N_\gamma - 1\}$ satisfying (3.11). If there exists such an i_0 uniquely, then set

$$x^* = y - \xi_{i_0}.$$

If there exist several i satisfying (3.11), choose i_0 as that minimizes

$$i \mapsto \gamma(\overline{x}_i^* - z) + \frac{1}{2}|\overline{x}_i^* - y|^2 \quad \text{subject to (3.11)},$$

where $\overline{x}_i^* = y - \xi_i$.

3.3. Algorithm and discretization

We begin by outlining the key steps in Algorithm 1. First, we set up the initial datum $u_0 \in C(\overline{W})$ and θ for a given initial curve Σ_0 and its orientation of the evolution. Accordingly, the function u_{n+1} for $n \geq 0$ is determined by

$$u_{n+1} := \arg\min_{w} E(w; u_n).$$

Then, we obtain the sequence of functions u_n and then the curves Σ_n approximating a solution $\Sigma(t_n)$ at $t_n = nh$ by

$$\Sigma_n := \left\{x \in \overline{W} : u_n(x) - \theta(x) \equiv 0 \mod 2\pi\mathbb{Z}\right\}. \tag{3.13}$$

In the algorithm, one can find the following two loops:

Outer loop. Finding (w^{k+1}, d^{k+1}) from (w^k, d^k) by (3.1)–(3.3).

Inner loop. Finding $(w^k_{\ell+1}, d^k_{\ell+1})$ from (w^k_ℓ, d^k_ℓ) by (3.4)–(3.6).

In these loops, we compute the functional

$$\begin{aligned} F^k_\mu(w, d; g) &:= F(w, d) + \frac{\mu}{2}\|d - \nabla w - b^k\|^2_{L^2} \\ &= \int_W \gamma(d - \nabla\theta)dx - \int_W f w dx + \frac{1}{2h}\left\|\frac{w - g}{\sqrt{\psi}}\right\|^2_{L^2} \\ &\quad + \frac{\mu}{2}\|d - \nabla w - b^k\|^2_{L^2} \end{aligned}$$

to check if the functions (w^k_ℓ, d^k_ℓ) or (w^k, d^k) reach the desired minimizer in the inner or outer loop, respectively. Here, $\psi = \gamma(\nabla(u_n - \theta))$, which may be zero in the computation. To avoid the division by zero in Algorithm 1, we introduce an approximation of F^k_μ of the form

$$\begin{aligned} F^k_{\mu,\alpha}(w, d; g) := &\int_W \gamma(d - \nabla\theta)dx - \int_W f w dx + \frac{1}{2h}\left\|\frac{w - g}{\sqrt{\max\{\psi, \alpha\}}}\right\|^2_{L^2} \\ &+ \frac{\mu}{2}\|d - \nabla w - b^k\|^2_{L^2} \end{aligned}$$

Algorithm 1: Minimizing movements of spiral curves

Input: $\Sigma_0 \subset \overline{W}$ and $u_0 \in C(\overline{W})$ such that $\Sigma_0 = \{u_0 - \theta \equiv 0\}$.
Output: $\Sigma(T) = \{u(T) - \theta \equiv 0\}$ with some function $u(T)\colon \overline{W} \to \mathbb{R}$.
(Time step) **for** $n = 0, 1, \dots, [T/h] - 1$ **do**
    Set $g = u_n$;
    Initialize $w^0 = u_n$, $b^0 = d^0 = 0$;
    (Outer loop) **for** $k = 0, 1, \dots$ **do**
        Initialize $w_0^k = w^k$, $d_0^k = d^k$;
        (Inner loop) **for** $\ell = 0, 1, 2, \dots$ **do**
            Solve (3.7)–(3.8) with $\psi = \gamma(\nabla(u_n - \theta))$ to obtain $w_{\ell+1}^k$;
            Calculate $d_{\ell+1}^k$ with Scheme (Sh);
            if $|F_{\mu,\alpha}^k(w_{\ell+1}^k, d_{\ell+1}^k; g) - F_{\mu,\alpha}^k(w_\ell^k, d_\ell^k; g)| < \varepsilon_{\mathrm{in}}$ **then** break;
        Set $w^{k+1} = w_{j+1}^k$, $d^{k+1} = d_{j+1}^k$;
        Set $b^{k+1} = b^k + \nabla w^{k+1} - d^{k+1}$;
        if $|F_{\mu,\alpha}^k(w^{k+1}, d^{k+1}; g) - F_{\mu,\alpha}^k(w^k, d^k; g)| < \varepsilon_{\mathrm{out}}$ **then** break;
    Set $u_{n+1} = w^{k+1}$;

with a positive constant $\alpha \ll 1$. In summary, we check if

$$\begin{cases} \text{(for inner)} & |F_{\mu,\alpha}^k(w_{\ell+1}^k, d_{\ell+1}^k; u_n) - F_{\mu,\alpha}^k(w_\ell^k, d_\ell^k; u_n)| < \varepsilon_{\mathrm{in}}, \\ \text{(for outer)} & |F_{\mu,\alpha}^k(w^{k+1}, d^{k+1}; u_n) - F_{\mu,\alpha}^k(w^k, d^k; u_n)| < \varepsilon_{\mathrm{out}} \end{cases}$$

for some $\varepsilon_{\mathrm{in}}, \varepsilon_{\mathrm{out}} \ll 1$ to break the inner and outer loop.

On the discretization, we apply the finite difference method. Note that $\nabla\theta$ should be considered as a smooth branch of it around the point $x_{i,j}$ at where we discretize the equations or functionals. See [31] for the details to avoid the discontinuity of θ in the computation. The boundary value problem given by (3.7)–(3.8) can be solved easily, for example, by the SOR method.

3.4. Discretization of the partial derivatives on a grid

We now summarize the discretization of $\psi = \gamma(\nabla(u_n - \theta))$ in (3.7) for Algorithm 1. In fact, one can find that (3.7) implies $w = g$ when $\gamma(\nabla(g - \theta)) = 0$. This fact may cause unexpected motions. For example, a small closed curve does not vanish even though it should be shrunk because of the curvature. Such an unexpected motion often appears when we approximate $\nabla(g - \theta)$ by the usual central difference. To avoid such a situation, we introduce an upwind difference for $\gamma(\nabla(g - \theta))$ as follows.

For simplicity of notation, we set $G_{i,j} = g(x_{i,j}) - \theta(x_{i,j})$ with $x_{i,j} = (i\Delta x, j\Delta x)$ for a uniform grid spacing $\Delta x > 0$. We present two upwind difference formulas; the first one is of the form

$$\widehat{\partial}_x^{\pm} G_{i,j} = \pm\Big\{\frac{G_{i\pm1,j} - G_{i,j}}{\Delta x} - \frac{\Delta x}{2}\sigma\Big(\frac{G_{i\pm2,j} - 2G_{i\pm1,j} + G_{i,j}}{\Delta x^2}, \frac{G_{i+1,j} - 2G_{i,j} + G_{i-1,j}}{\Delta x^2}\Big)\Big\},$$

where

$$\sigma(p,q) = \begin{cases} p & \text{if } |p| < q, \\ q & \text{otherwise.} \end{cases}$$

The second one is just a usual difference in the form

$$\widetilde{\partial}_x^{\pm} U = \pm\frac{G_{i\pm1,j} - G_{i,j}}{\Delta x}.$$

Then, we define

$$\partial_x^{\pm} G_{i,j} = \begin{cases} \widehat{\partial}_x^{\pm} G_{i,j} & \text{if } x_{i\pm1,j} \in W \text{ and } x_{i,j\pm1} \in W, \\ \widetilde{\partial}_x^{\pm} G_{i,j} & \text{otherwise.} \end{cases}$$

Note that $G_{i\pm1,j}$ in $\widetilde{\partial}_x^{\pm} G_{i,j}$ (resp. $G_{i\pm2,j}$ in $\widehat{\partial}_x^{\pm} G_{i,j}$) is calculated by extension of $G_{i,j}$ with the Neumann boundary condition if $x_{i\pm1,j} \notin W$ (resp. $x_{i\pm2,j} \notin W$). We also define $\partial_y^{\pm} G_{i,j}$ with the similar manner of the above. Note that we use $\widetilde{\partial}_x^{\pm} G_{i,j}$ in this paper even when $x_{i,j\pm1} \notin W$. We use the same order of the approximation of $\partial_x(g-\theta)$ and $\partial_y(g-\theta)$.

We now introduce the approximation formula of $\psi = \gamma(\nabla(g-\theta))$. For $q = (q^1, q^2) \in \mathbb{R}^2 \setminus \{0\}$, let us set

$$(q \cdot \nabla(g-\theta))_{i,j} = \begin{cases} q^1\partial_x^+ G_{i,j} + q^2\partial_y^+ G_{i,j} & \text{if } q^1 \geq 0,\ q^2 \geq 0, \\ q^1\partial_x^- G_{i,j} + q^2\partial_y^+ G_{i,j} & \text{if } q^1 < 0,\ q^2 \geq 0, \\ q^1\partial_x^+ G_{i,j} + q^2\partial_y^- G_{i,j} & \text{if } q^1 \geq 0,\ q^2 < 0, \\ q^1\partial_x^- G_{i,j} + q^2\partial_y^- G_{i,j} & \text{if } q^1 < 0,\ q^2 < 0. \end{cases} \tag{3.14}$$

Then, for $\gamma(p) = \max_{0\leq k\leq N_\gamma-1} n_k \cdot p$, we introduce the approximation $\psi_{i,j} \approx \gamma(\nabla(g-\theta)(x_{i,j}))$ in (3.7) for Algorithm 1 as

$$\psi_{i,j} = \max_{0\leq k\leq N_\gamma-1} (n_k \cdot \nabla(g-\theta))_{i,j}.$$

Hence, we obtain the difference equation for (3.7), which is of the form

$$w_{i,j} - h\mu\psi_{i,j}\Delta w_{i,j} = g_{i,j} + h\psi_{i,j}(f_{i,j} - \mu[\operatorname{div}(d_\ell^k - b^k)]_{i,j}),$$

where $\Delta w_{i,j}$ is the usual finite difference approximation of Δw at $x_{i,j}$.

4. Numerical results

We now apply the algorithm introduced in the previous sections to the evolution of spirals by (1.1) and propose some numerical results.

Throughout this section, we set the domain $\Omega = [-1.5, 1.5]^2$ with the Cartesian grid

$$D_\triangle = \left\{x_{i,j} = (i\Delta x, j\Delta x) \in \Omega : \frac{-1.5}{\Delta x} \le i, j \le \frac{1.5}{\Delta x}\right\}$$

for a uniform grid spacing Δx. We will set $\Delta x = 0.02/s$ with $s = 1, 2, 3, 4, 5$ to examine the numerical accuracy of our algorithms in Section 4.1, and often visualize the spiral profiles for $s = 3$.

We will further assume that the centers of the spirals lie on the grid nodes, that is, $a_\ell \in D_\triangle$ for every $\ell = 1, 2, \dots, N$. As in the definition of W, we will exclude the grid nodes $x_{i,j}$ such that

$$|x_{i,j} - a_\ell| < r = 2\Delta x$$

to avoid the complexity of computations around the centers a_ℓ, $\ell = 1, 2, \dots, N$.

The evolution equation in (1.1) is rephrased in this section as

$$V_\gamma = v_\infty(1 - \rho_c \kappa_\gamma) \tag{4.1}$$

for consistency with [31, 32] and [8], where v_∞ and ρ_c are positive constants. Here, we consider only a constant driving force. By considering $\tilde{f} = v_\infty$ and $\tilde{\gamma} = v_\infty \rho_c \gamma$ instead of f and γ in (1.1), we can apply the algorithms as in the previous sections to (4.1).

4.1. Unit spiral

In this section we consider the fundamental case, that is, a single center with a single spiral. Let $N = 1$, $a_1 = 0$, $m_1 = 1$ and thus we set $\theta(x) = \arg x$. We choose the size of the center as $r = 2\Delta x$. We present numerical studies for the case corresponding to a triangular spiral; this means $N_\gamma = 3$ and

$$n_j = 2\left(\cos\frac{\pi(2j+1)}{3}, \sin\frac{\pi(2j+1)}{3}\right), \quad \text{for } j = 0, 1, 2. \tag{4.2}$$

Note that, in this case, $\gamma^\circ(p) = \max_{0 \le j \le 2} \tilde{n}_j \cdot p$ with

$$\tilde{n}_j = \left(\cos\left(\frac{2\pi j}{3}\right), \sin\left(\frac{2\pi j}{3}\right)\right).$$

(See [21] for details of the calculation of γ° from γ.) We examine the proposed algorithm for

$$V_\gamma = 1 - 0.01\kappa_\gamma \quad (v_\infty = 1,\ \rho_c = 0.01);$$

the time interval is $[0, 0.8]$ with time span $h = 0.04\Delta x$. The other parameters for the presented computational results are μ, ε_{in}, ε_{out}, α as follows:

$$\mu = v_\infty \rho_c, \quad \varepsilon_{\text{in}} = 10^{-2} v_\infty \rho_c, \quad \varepsilon_{\text{out}} = 10^{-5} v_\infty \rho_c, \quad \alpha = 10^{-8}.$$

We compare the numerical results computed by our algorithm with those by the front-tracking model introduced in [20]. A brief review of the front-tracking model is provided in Appendix A.

We will use two functions to quantify the difference between the spirals computed by our algorithm and those from the front-tracking approach. We denote the spiral computed by Algorithm 1 as $\Sigma_h(t)$ and the one computed by the front-tracking method as $\Sigma_\mathrm{d}(t)$.

The first one, $\mathcal{D}(t)$ is based on the distance function to Σ_h. Let $d_{\Sigma_h}(t,x)$ be a distance function from $\Sigma_h(t)$ with the usual Euclidean metric. Then,

$$\mathcal{D}(t) = \sup\left\{d_{\Sigma_h}(t,x) : x \in \Sigma_\mathrm{d}(t)\right\}$$

expresses the distance between $\Sigma_h(t)$ and $\Sigma_\mathrm{d}(t)$.

The second one, denoted by $\mathcal{A}(t)$ (and defined in (4.3) below), measures the area of the interposed region by $\Sigma_\mathrm{d}(t)$ and $\Sigma_h(t)$. This concept is introduced in [21]. The function $\mathcal{A}$ involves the height function of the crystal surfaces. Let $H_{\Sigma_h}(t,x)$ and $H_{\Sigma_\mathrm{d}}(t,x)$ denote the height functions corresponding to $\Sigma_h(t)$ and $\Sigma_\mathrm{d}(t)$ (as defined in [21]).

For $\Sigma_h(t)$ given by (3.13), we prepare the principal value $\widehat{\theta}(x) = \arg x \in [-\pi,\pi)$, and let $\zeta(t,x) \in \mathbb{Z}$ be such that

$$2\pi\zeta(t,x) < u_n(x) - \widehat{\theta}(x) \le 2\pi(\zeta(t,x)+1)$$

for $(t,x) \in [0,\infty) \times \overline{W}$. Then,

$$\theta_h(t,x) = \widehat{\theta}(x) + 2\pi\zeta(t,x)$$

yields the branch of $\arg x$ whose discontinuities are only on $\Sigma_h(t)$.

For $H_{\Sigma_\mathrm{d}}(t)$, let

$$\mathbf{N}_j = \frac{\widetilde{n}_j}{|\widetilde{n}_j|}, \quad \mathbf{T}_j = \begin{pmatrix} 1 & 0 \\ 0 & -1 \end{pmatrix} \mathbf{N}_j \quad \text{for } j \in \mathbb{Z}/(N_\gamma\mathbb{Z})$$

denote the outer unit normal and tangential vector of j-th facet of $\mathcal{W}_\gamma$ with the extended facet number $j \in \mathbb{Z}/(N_\gamma\mathbb{Z})$. We now consider a polygonal curve $\Sigma_\mathrm{d}(t) = \bigcup_{j=0}^{k} \Sigma_{\mathrm{d},j}(t)$ given by

$$\Sigma_{\mathrm{d},j}(t) = \begin{cases} \left\{(1-\sigma)y_j(t) + \sigma y_{j-1}(t) : \sigma \in [0,1]\right\} & \text{if } j = 1,2,\dots,k, \\ \left\{y_0(t) + \sigma\mathbf{T}_0 : \sigma \ge 0\right\} & \text{if } j = 0 \end{cases}$$

with its vertices $\{y_j(t) : j = 0,\dots,k\}$. Note that

$$\frac{y_{j-1}(t) - y_j(t)}{|y_{j-1}(t) - y_j(t)|} = \mathbf{T}_j$$

and then all facets of $\Sigma_\mathrm{d}(t)$ are parallel to those of $\mathcal{W}_\gamma$. (See (A.1)–(A.3) and Appendix A for details on how to determine $y_j(t)$.) Let $\widetilde{\vartheta}^* = \widetilde{\vartheta}_k - \pi/2$, that is, $(\cos\widetilde{\vartheta}^*, \sin\widetilde{\vartheta}^*) = \mathbf{T}_k$.

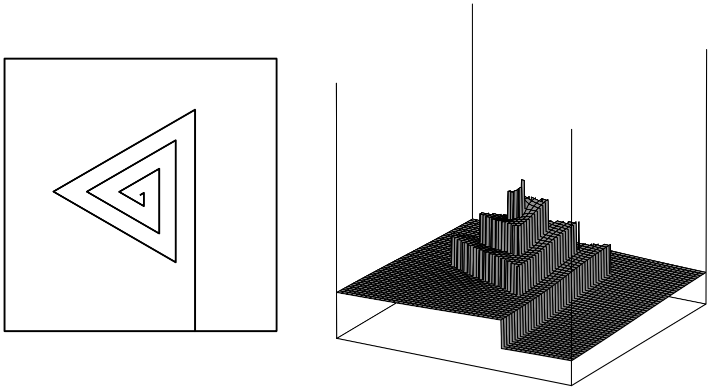

Figure 1. Spiral step function $H_{\Sigma_{\mathrm{d}}}$.

We first prepare a branch of $\arg x$ denoted by $\Theta_{\mathrm{d}}(t,x) \in (\widetilde{\vartheta}^* - 2\pi, \widetilde{\vartheta}^*]$ whose discontinuity is only on a half line including $\Sigma_{\mathrm{d},k}(t)$. Let

$$D_j(t) = \left\{x \in \mathbb{R}^2 : (x - y_j) \cdot \mathbf{N}_j > 0\right\}$$

for $j = 0, \ldots, k$, which denotes the region including the terrace in front of $\Sigma_{\mathrm{d},j}(t)$. Then,

$$\theta_{\mathrm{d}}(t,x) = \Theta_{\mathrm{d}}(t,x) - 2\pi \sum_{j=1}^{k} \chi(x; D_j^c(t) \cap D_{j-1}(t))$$

yields the branch of $\arg x$ whose discontinuities are only on $\Sigma_{\mathrm{d}}(t)$, where

$$\chi(x;U) = \begin{cases} 1 & \text{if } x \in U, \\ 0 & \text{otherwise} \end{cases}$$

for $U \subset \mathbb{R}^2$. Hence,

$$H_{\Sigma_{\mathrm{d}}}(t,x) = \frac{1}{2\pi}\theta_{\mathrm{d}}(t,x), \quad H_{\Sigma_h}(t,x) = \frac{1}{2\pi}\theta_h(t,x)$$

yield the surface height functions of $\Sigma_{\mathrm{d}}(t)$ (resp. $\Sigma_h(t)$), which have 1-jump discontinuity on $\Sigma_{\mathrm{d}}(t)$ (resp. $\Sigma_h(t)$). Figure 1 is an example of H_{Σ_d}.

Now, set up the initial data so that $H_{\Sigma_d} = H_{\Sigma_h}$ at $t = 0$. Then, the function $|H_{\Sigma \mathrm{d}}(t,x) - H_{\Sigma_h}(t,x)|$ plays the role of a characteristic function of the interposed region between $\Sigma_{\mathrm{d}}(t)$ and $\Sigma_h(t)$ with multiplicity. (An example of the graph of $|H_{\Sigma_{\mathrm{d}}}(t,x) - H_{\Sigma_h}(t,x)|$ is shown in Figure 2.) Hence, we define

$$\mathcal{A}(t) = \frac{1}{|W|}\int_W |H_{\Sigma_{\mathrm{d}}}(t,x) - H_{\Sigma_h}(t,x)|dx. \tag{4.3}$$

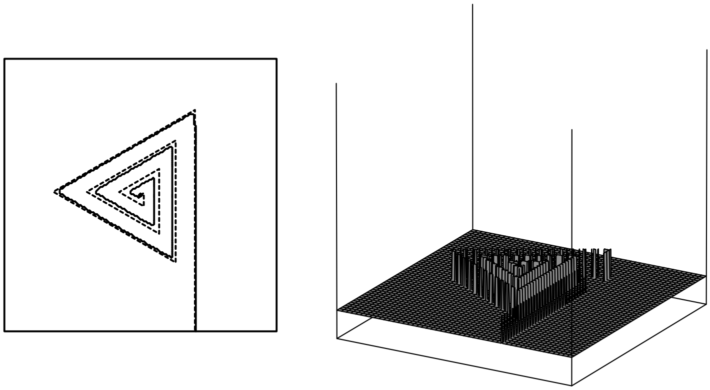

Figure 2. Graph of $|H_{\Sigma_\mathrm{d}} - H_{\Sigma_h}|$. In the left panel, the dashed and solid lines indicate $\Sigma_\mathrm{d}(t)$ and $\Sigma_h(t)$, respectively.

This quantity indicates the difference between $\Sigma_h(t)$ and $\Sigma_\mathrm{d}(t)$ by area of the interposed region.

We take the opportunity to provide some additional mathematical exposition on $\mathcal{A}(t)$. Following [28], we introduce a covering space $\mathfrak{X}$ of the form

$$\mathfrak{X} = \Big\{(x,\xi) \in \overline{W} \times \mathbb{R}^N : \xi = (\xi_1, \dots, \xi_N) \text{ satisfies} \\ (\cos\xi_j, \sin\xi_j) = \arg\frac{x-a_j}{|x-a_j|} \text{ for } j = 1,2,\dots,N\Big\},$$

where a_j, $j = 1,2,\dots,N$, are the centers of the spirals. We then consider spiral curves on the Riemannian-like surface

$$\mathfrak{W} = \Big\{(x,z) \in \overline{W} \times \mathbb{R} : z = \frac{1}{2\pi}\sum_{j=1}^N m_j\xi_j,\ (x,\xi_1,\dots,\xi_N) \in \mathfrak{X}\Big\}.$$

In other words, the height function $H_{\Sigma_\mathrm{d}}(t,x)$ of $\Sigma_\mathrm{d}(t)$ divides $\mathfrak{W}$ into the inside of $\Sigma_\mathrm{d}(t)$ of the form

$$\widetilde{I}_\mathrm{d}(t) = \big\{(x,\xi) \in \mathfrak{W} : \xi \le H_{\Sigma_\mathrm{d}}(t,x)\big\},$$

and the outside as $\mathfrak{W} \setminus \widetilde{I}_\mathrm{d}(t)$. We here define $\widetilde{I}_h(t)$, the inside of $\Sigma_h(t)$, in the same manner as with $\Sigma_h(t)$ and $H_{\Sigma_h}(t,x)$. Then, *the interposed region between $\Sigma_\mathrm{d}(t)$ and $\Sigma_h(t)$* indicates $\widetilde{I}_h(t)\triangle\widetilde{I}_\mathrm{d}(t) = (\widetilde{I}_h(t) \setminus \widetilde{I}_\mathrm{d}(t)) \cup (\widetilde{I}_\mathrm{d}(t) \setminus \widetilde{I}_h(t))$. The quantity $\mathcal{A}(t)$ computes the area of $\widetilde{I}_h(t)\triangle\widetilde{I}_\mathrm{d}(t)$ in the sense of the usual Lebesgue measure in $\mathbb{R}^2$. Moreover, note that $\mathcal{A}(t)$ includes the multiplicity of the interposed region. In fact, let us consider the situation $W = \{x \in \mathbb{R}^2 : \rho \le |x| \le R\}$ for some $R > \rho > 0$, $\theta(x) = \arg x$, $\Sigma_\mathrm{d}(t) = \Sigma_h(t) = \{x = (x_1,0) \in \overline{W} : x_1 > 0\}$, but $\widetilde{I}_\mathrm{d} = \{(x,\xi) \in \mathfrak{W} : \xi \le 0\}$, $\widetilde{I}_h = \{(x,\xi) \in \mathfrak{W} : \xi \le 2\}$.

In this case $\mathcal{D}(t) = 0$. *At first glance, it might seem that the area of* $\{x \in \overline{W} : (x, \xi) \in \widetilde{I}_h(t) \triangle \widetilde{I}_{\mathrm{d}}(t)\}$ *is zero, but* $\mathcal{A}(t) = 2$ *(twice* $|W|$*).*

We provide several numerical results verifying the accuracy of our scheme. In the following examinations, we set up the initial curve as

$$\Sigma_{\mathrm{d}}(0) = \Sigma_h(0) = \big\{\sigma \mathbf{T}_0 : \sigma \in [0, \infty)\big\}.$$

Accordingly, we set the initial data as

$$\text{The front-tracking model} : k = 1,\ d_1(0) = 0.$$
$$\text{Algorithm 1} : u_0 = -\frac{\pi}{2}.$$

In this paper, the solution $\Sigma_{\mathrm{d}}(t)$ by the front-tracking model is obtained by solving the ODE system (A.4) with a fourth-order Runge–Kutta method and smaller time span $\Delta t = 10^{-6}$ than that of our approach. Then, we compute the height function $H_{\Sigma_{\mathrm{d}}}(t, x)$ by the solution of front-tracking model. Figure 3 displays overlapped snapshots of the evolving spirals computed using the front-tracking model and using Algorithm 1 at $t = 0, 0.4, 0.6$, and 0.8, for the case (4.2). In Figure 4 we show the graphs of $\mathcal{D}(t)$ and $\mathcal{A}(t)$ under the above settings. One can find that the difference becomes smaller when we choose smaller Δx (higher s). However, both $\mathcal{D}(t)$ and $\mathcal{A}(t)$ increase with respect to t for all cases. From Figure 3, these differences arise and develop around the center when the facet associated with the center turns around the direction of their evolution. On the other hand, one also finds that the graphs of $\mathcal{D}(t)$, in particular when $s = 1$ or 2, seem to be concave even when the graphs of $\mathcal{A}(t)$ in the same cases are convex. This seems to be the situation in which the difference between the two simulations around the center becomes too large so that the step from the front-tracking model catches up with some other portion of the steps by Algorithm 1.

Next, we investigate the number of inner and outer loops as the computational cost of our approach. Figure 5 presents the numbers of outer loops for each time step. We find that the number of outer loops in a time step ranges from 20 to 80. On the other hand, Figure 6 present the graphs of average numbers of inner loops par one outer loop for each time step. We find that the range of inner loops is from 1 to 1.5 in all cases. In particular, the number of inner and outer loops seem to remain very similar for the different values of Δx used in the study.

We here give some remarks on numerical computation. For the level set equation in (2.6), the fully explicit finite difference method is a simple approach to compute it; see [21] for details. Our numerical results in this paper are close to those in [21]. It is well known that we often set the time span as $h = O(\Delta x^p)$. For the level set equation for crystalline curvature, we shall choose $p \geq 2$ for stable and highly accurate computation when we choose smaller Δx. On the other hand, in our approach we can set $h = O(\Delta x)$ $(p = 1)$, which is an advantage for computation with smaller Δx. However, our approach has a lot of numerical parameters affecting numerical accuracy. In particular, μ affects

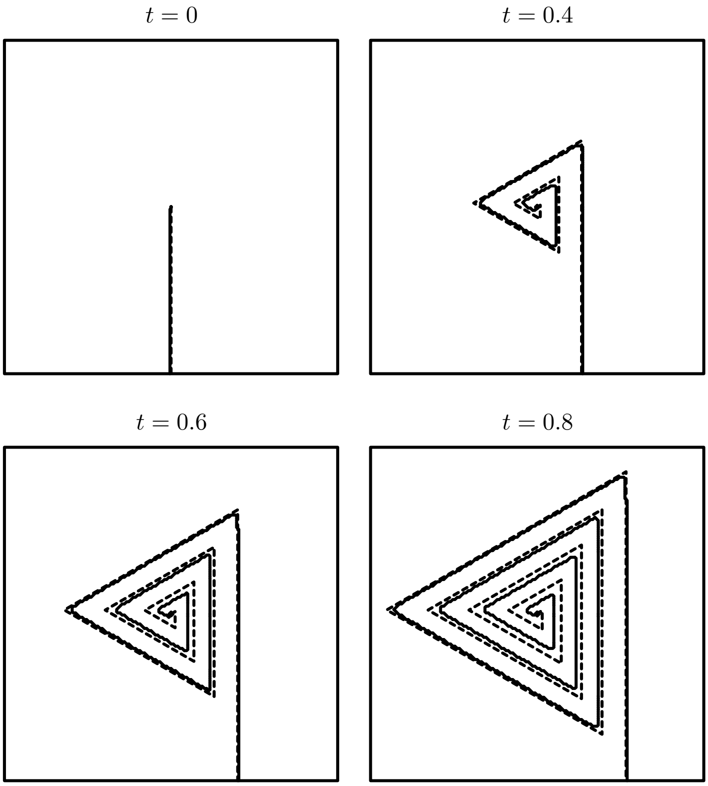

Figure 3. Overlapping snapshots of two spirals at $t = 0, 0.4, 0.6$, and 0.8, computed using the front-tracking model (dashed curves) and Algorithm 1 (solid curves), with $\Delta x = 1/150$ ($s = 3$).

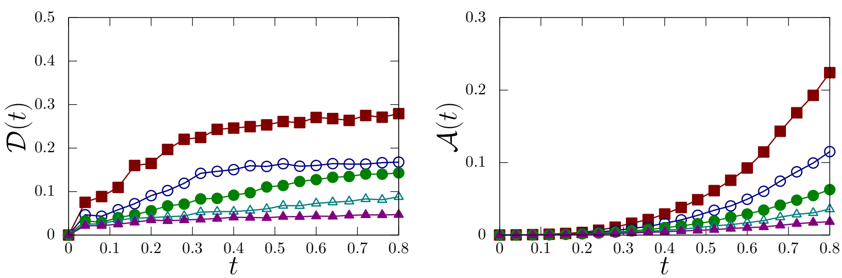

Figure 4. Graphs of the distances $\mathcal{D}(t)$ and the area difference $\mathcal{A}(t)$ between the spirals computed using the front-tracking model and Algorithm 1. The lines with ■, ∘, •, △, ▲ correspond to the cases of $s = 1, 2, 3, 4, 5$, respectively.

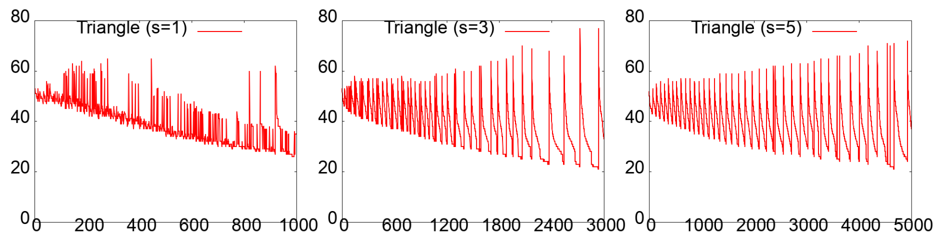

Figure 5. The number of outer loops used in the simulations involving three different values of s. The horizontal axis reveals the number of time steps performed in the evolution, while the vertical axis shows the number of outer loops.

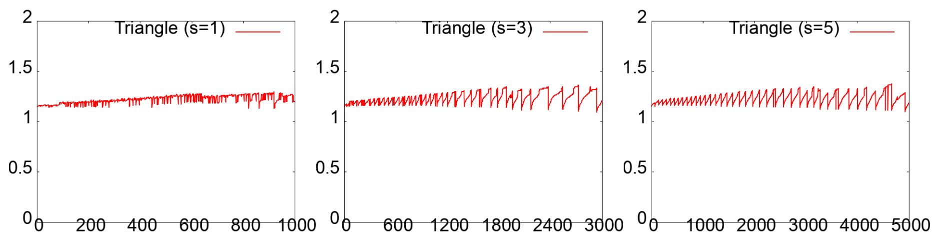

Figure 6. The number of inner loops used in the simulations involving three different values of s. The horizontal axis reveals the number of time steps performed in the evolution and the vertical axis shows the average number of inner loops per outer loop.

the profile of spirals and numerical costs. In Figure 3 one can find that the solution of our approach has smoothing effect, particularly around the corner of the polygonal curve. If one wants to obtain sharp corner in the solution, one option is to set μ to be smaller. However, if we do so, the number of inner and outer loops may increase.

Here we also give some remarks on the comparison between the front-tracking model and our approach. For the computation of the evolution of a single spiral, the front-tracking model is extremely quick to obtain the solution $\Sigma_{\mathrm{d}}(t)$. If we compute the height function $H_{\Sigma_{\mathrm{d}}}(t,x)$, almost all of the computation time is spent to compute $H_{\Sigma_{\mathrm{d}}}(t,x)$ from $\Sigma_{\mathrm{d}}(t)$. Moreover, the front-tracking approach requires generating new facets, so the ODE system (A.4) and thus the facet number k becomes larger in time. Thus, the computational time of the front-tracking model for one time step increases, although that of our approach seems to be constant.

We conclude this subsection by presenting a numerical result of the case of a single center with multiple spirals. Figure 7 presents the profiles of triple spirals evolving by

$$V = 2(1 - 0.04\kappa_\gamma), \tag{4.4}$$

$$\gamma(p) = |p^1| + |p^2|,\ \gamma^\circ(p) = \max\{|p^1|, |p^2|\},\ p = (p^1, p^2) \in \mathbb{R}^2 \tag{4.5}$$

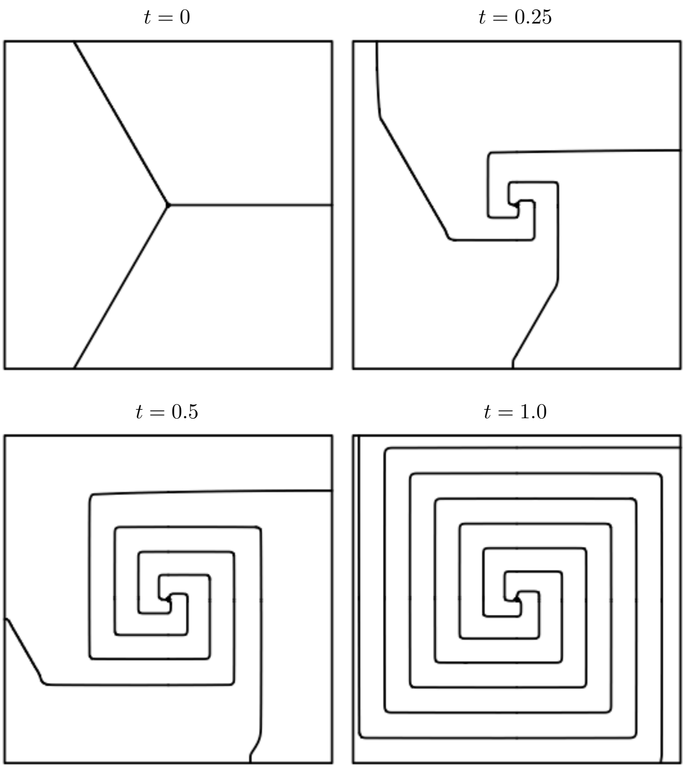

Figure 7. Profiles of triple spirals evolving by (4.4) and (4.5) from a single center at $t = 0$, $t = 0.25$, $t = 0.5$, and $t = 1$.

with $N = 1$, $a_1 = 0$, and $m_1 = 3$, and thus $\theta = 3 \arg x$. In our earlier work [29], an approach using a signed distance function in a neighborhood of spirals is investigated. However, it is difficult to apply that approach in this situation.

Remark 4.1. According to the front-tracking model [20], the facet associated with the center (center-facet) is stationary if it is shorter than the critical length. The critical length in question is the length of the facet of $\mathcal{W}_\gamma$ facing the same direction as the center facet. When the length of the center-facet reaches the critical length, a new facet is generated at the center, and the newly generated facet becomes the center-facet. Our approach does not have such a generation rule. However, the behavior of the facet around the center for our algorithms is very similar to the generation rule outlined in [20].

Figure 8 show a superposition of snapshots of a spiral evolving with

$$V = 4(1 - 0.2\kappa_\gamma), \tag{4.6}$$

and (4.5) by Algorithm 1. The dashed line is $x = \pm(0.4 + r)$, $y = \pm(0.4 + r)$. The initial curve is $\{(x, 0) : x > 0\}$.

We now consider the same situation with the front-tracking model. Then, the initial data is $\Sigma_{\mathrm{d}}(0) = \Sigma_{1,\mathrm{d}}(0) \cup \{(x, 0) : x \geq 0\}$, $\Sigma_{1,\mathrm{d}}(t) = \{(0, y) : 0 \leq y \leq d_1(t)\}$ and $d_1(0) = 0$. For the evolution equation (4.6) with (4.5), we find $\mathcal{W}_\gamma = [-0.2, 0.2]^2$ in this case so that the center-facet $\Sigma_{1,\mathrm{d}}(t)$ can move after the time $t^* > 0$ when $d_1(t^*) = 0.4$. In other words, $\Sigma_{\mathrm{d}}(t)$ evolves as follows:

(1) First, the initial horizontal line $\{(x, 0) : x \geq 0\}$ moves upwards, yielding $\Sigma_{0,\mathrm{d}}(t) = \{(x, d_1(t)) : x \geq 0\}$, while being connected to the center by the vertical line $\Sigma_{1,\mathrm{d}}(t) = \{(0, y) : 0 \leq y \leq d_1(t)\}$ while $d_1(t) < 0.4$.

(2) When $d_1(t) = 0.4$, the new facet $\Sigma_{2,\mathrm{d}}(t) = \{(x, 0) : -d_2(t) \leq x \leq 0\}$ is generated. The center facet of $\Sigma_{\mathrm{d}}(t)$ is changed from $\Sigma_{1,\mathrm{d}}(t)$ to $\Sigma_{2,\mathrm{d}}(t)$, and then $\Sigma_{1,\mathrm{d}}(t)$ can move as $\Sigma_{1,\mathrm{d}}(t) = \{(-d_2(t), y) : 0 \leq y \leq d_1(t)\}$.

The motion of $\Sigma_h(t)$ is similar to the above scenario. The vertical line in Figure 8 moves very slowly until the horizontal line reaches the dashed line ($y = 0.4 + r$). After the horizontal line goes over the dashed line, the vertical line accelerates. This seems to be the reason why we observe that $\Sigma_{\mathrm{d}}(t)$ and $\Sigma_h(t)$ are very close in a numerical sense.

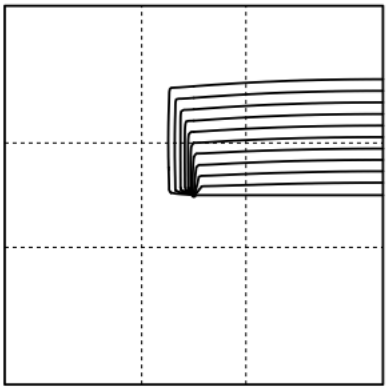

Figure 8. Serial picture of an evolving spiral from $t = 0$ to $t = 0.25$ per $\Delta t = 0.025$, whose center is the origin, by (4.6) and (4.5). The dashed lines denote $x = \pm(0.4 + r)$ and $y = \pm(0.4 + r)$.

4.2. Merging of spirals

Co-rotating and opposite rotational pairs are given by setting

$$\theta(x) = m_1 \arg(x - a_1) + m_2 \arg(x - a_2);$$

set $m_1 m_2 > 0$ for a co-rotating pair, or $m_1 m_2 < 0$ for an opposite rotational pair. Figure 9 shows the profiles of co-rotating spirals at $t = 0$, 0.25, 0.39, 0.40, 0.50, and 1.0 evolving

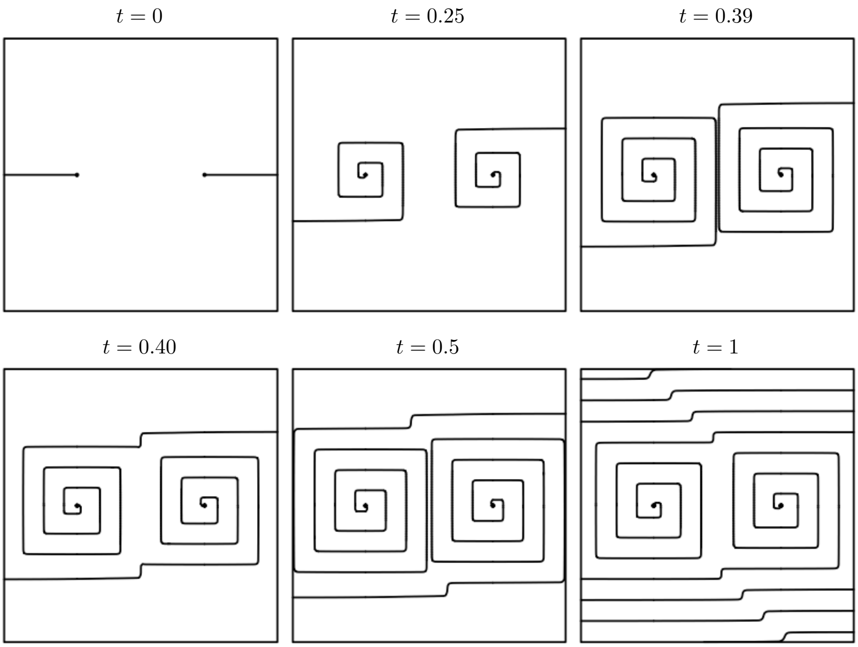

Figure 9. Profiles of co-rotating spirals at $t = 0$, 0.25, 0.39, 0.40, 0.5, and 1.0 evolving by (4.7) with Algorithm 1. Note that $\Delta x = 1/150$ ($s = 3$).

by

$$V = 2(1 - 0.1\kappa_\gamma), \tag{4.7}$$

with γ defined in (4.5). The other parameters are as follows:

- Centers: $a_1 = (-0.7, 0)$, $a_2 = (0.7, 0)$, $m_1 = m_2 = 1$.
- Initial curve: $\Sigma_0 = \{a_1 + (-x, 0) \in \overline{W} : x > 0\} \cup \{a_2 + (x, 0) \in \overline{W} : x > 0\}$, and thus $u_0(x) = 0$.

The panels of $t = 0.39$ and 0.40 in Figure 9 show the detailed profiles when the spirals merge. Our approach can keep very narrow parallel facing steps just before merging, at $t = 0.39$. It means that our approach has a good performance to reduce the unwanted smoothing effect. Note that $\nabla(u - \theta) = 0$ where facing steps merge. Thus, one may find that an unexpected hole (closed curve whose direction is inside of the curve) remains in such a situation, in particular when we use the usual central difference for the computation of $\psi = \gamma(\nabla(u_n - \theta))$ in Algorithm 1. We use the higher-order upwind discretization (3.14) to avoid this unwanted effect.

In the works [3, 19, 20, 37], the solution is defined in a class of admissible polygonal curves, which satisfy

- There is no self-intersection.
- If a facet of the curve has the same direction as the normal $\mathbf{n} = \mathbf{N}_j$ as the j-th facet of $\mathcal{W}_\gamma$, its adjacent facet has the direction of a normal either $\mathbf{n} = \mathbf{N}_{j-1}$ or $\mathbf{n} = \mathbf{N}_{j+1}$.

The second property of the above is required to define the crystalline curvature for $\mathcal{W}_\gamma$. However, the merging of spirals make break the admissibility of the curve, even though each facets of merged spiral are parallel to some facet of $\mathcal{W}_\gamma$. Figure 10 shows profiles of co-rotating pentagonal spirals at $t = 0, 0.2, 0.4$, and 0.6 evolving by

$$\begin{cases} V_\gamma = 3(1 - 0.01\kappa_\gamma), \\ \text{with} \quad \gamma(p) = \max\limits_{0 \le j \le 4} n_j \cdot p, \quad n_j = \left(\cos\dfrac{\pi(2j+1)}{5}, \sin\dfrac{\pi(2j+1)}{5}\right). \end{cases} \tag{4.8}$$

The two centers are at $a_1 = (-1, 0.4)$ and $a_2 = (1, -0.4)$ with $m_1 = m_2 = 1$. Note that the above situation provides a regular pentagonal $\mathcal{W}_\gamma$ whose facet has the normal $\mathbf{N}_j = (\cos(2\pi j/5), \sin(2\pi j/5))$ for $j = 0, 1, 2, 3, 4$. We choose the initial curve as

$$\Sigma_0 = \left\{a_1 + \sigma\mathbf{T}_0 : \sigma > 0\right\} \cup \left\{a_2 + \sigma\mathbf{T}_2 : \sigma > 0\right\}. \tag{4.9}$$

In this situation, a vertex of the curve provided from a_2 touches to the flat portion of the curve from a_1 between $t = 0.2$ and $t = 0.4$. At that time, the curve is divided into two parts, which are the merging curves between the facets parallel to $\mathbf{T}_0$ and $\mathbf{T}_2$, or $\mathbf{T}_0$ and $\mathbf{T}_3$. Hence, one can find that merging spirals may fail to satisfy the second requirement of the admissibility condition. In such cases, the ODE approach due to [20] needs a procedure adding several zero-length facets fulfilling admissibility; see [14, 15, 27]. Such an intermediate facet also seems to appear in the evolving curve by our methods, although it is too hard to find in Figure 10. To clarify the behavior around the merging of spirals, we examine the situation

$$\begin{cases} V = 1 - 0.1\kappa_\gamma \quad \text{with the same anisotropy of (4.8)}, \\ a_1 = (-0.2, 1),\ a_2 = (0.2, -1),\ m_1 = m_2 = 1, \end{cases} \tag{4.10}$$

Figure 11 presents the profiles of the evolving curve by (4.10) with the same initial curve as (4.9). One can find that the intermediate facet parallel to $\mathbf{T}_1$ appears in the merging curves between the facets parallel to $\mathbf{T}_0$ and $\mathbf{T}_2$; see the panel of $t = 0.8$ or $t = 1$ in Figure 11.

4.3. Combination of anisotropy

Let us consider the situation such that the anisotropies of crystalline curvature and the eikonal term, which are denoted by γ_1 and γ_2, are possibly different. In other words, we now solve the level set equation of the form

$$u_t - \gamma_1(\nabla(u - \theta))\left\{\operatorname{div}[\xi_2(\nabla(u - \theta))] + f\right\} = 0 \quad \text{in } (0, T) \times W,$$

where $\xi_2 = \nabla\gamma_2$. For such an equation, our approach can easily be adapted as follows:

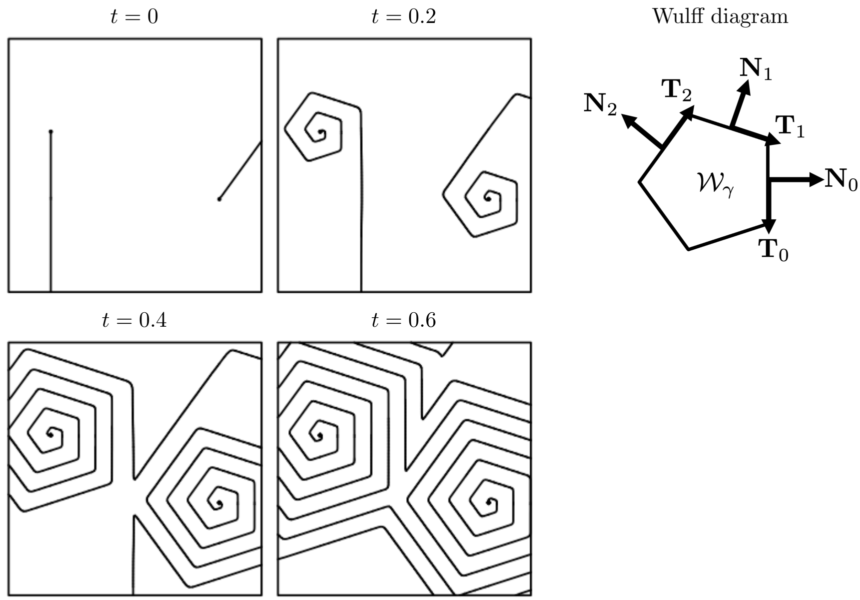

Figure 10. Profiles of co-rotating spirals evolving by (4.8) at $t = 0, 0.2, 0.4, 0.6$ with Algorithm 1, and the Wulff diagram $\mathcal{W}_\gamma$ of this case.

(1) Solve (3.7)–(3.8) with $\psi = \sqrt{\gamma_1(\nabla(u_n - \theta))}$.

(2) Solve (3.9) by the scheme (Sh) with $\gamma = \gamma_2$.

Figure 12 shows the profiles of a spiral at $t = 0$, 0.25, 0.50, and 1.0 evolving by

$$\begin{cases} V_1 = 2(1 - 0.01\kappa_2), \\ \gamma_1(p) = \max\limits_{0 \le j \le 4} n_{1,j} \cdot p, \\ \qquad n_{1,j} = \left(\cos \dfrac{\pi(2j+1)}{5}, \sin \dfrac{\pi(2j+1)}{5}\right), \\ \gamma_2(p) = \max\limits_{0 \le j \le 3} n_{2,j} \cdot p, \\ \qquad n_{2,j} = \sqrt{2}\left(\cos \dfrac{\pi(2j+1)}{4}, \sin \dfrac{\pi(2j+1)}{4}\right) \quad \text{(case (4.5))} \end{cases} \tag{4.11}$$

with Algorithm 1, where V_1 and κ_2 denotes the normal velocity defined by γ_1 and the crystalline curvature defined by γ_2, respectively. The Wulff diagrams $\mathcal{W}_1$ by γ_1 and $\mathcal{W}_2$ by γ_2 are respectively regular pentagon and square, whose facets have the following normal vectors:

$$\mathcal{W}_1 : \mathbf{N}_{1,j} = \left(\cos \frac{2\pi j}{5}, \sin \frac{2\pi j}{5}\right), \quad \mathcal{W}_2 : \mathbf{N}_{2,j} = \left(\cos \frac{\pi j}{2}, \sin \frac{\pi j}{2}\right).$$

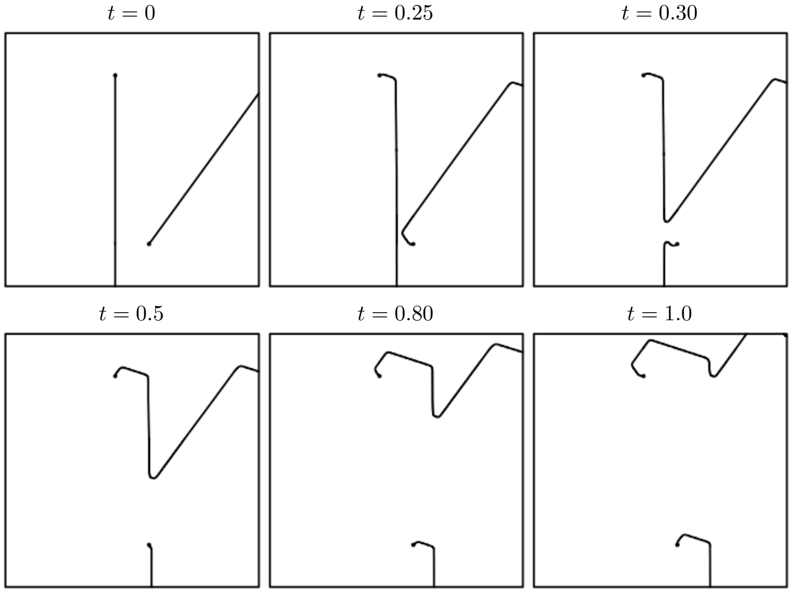

Figure 11. Profiles of merging spirals breaking admissibility. The setting of this situation is as in (4.10), and $\Delta x = 0.00667$ ($s = 3$).

Thus, the evolving spiral forms an octagonal polygonal curve whose normal directions are chosen from $\{\mathbf{N}_{1,j} : 0 \le j \le 4\} \cup \{\mathbf{N}_{2,j} : 0 \le j \le 3\}$. Yazaki [41] shows that a curve evolving by $V = -\kappa_\gamma + 1$ asymptotically converges to the solution of $V = 1$, after the curve has moved sufficiently far away. From the context of this result, the evolving spiral will show the profile as follows:

- It is close to the rescaling of $\mathcal{W}_2$ around the center.
- It becomes a convex polygonal curve whose normal directions are chosen from $\mathbf{N}_{1,j}$ or $\mathbf{N}_{2,j}$ in the intermediate region.
- Asymptotically, it is close to the rescaling of $\mathcal{W}_1$ on a far away region.

4.4. Interlace motion

Let us consider the situation such that all centers have the same multiple numbers of spirals, that is, $m_j = \widetilde{m}_j m_0$ with $\widetilde{m}_j \in \mathbb{Z}$ and $m_0 \ge 2$ for $j = 1, \dots, N$. Then, the level set description of spiral curves

$$\Sigma(t) = \left\{x \in \overline{W} : u(t,x) - \theta(x) \equiv 0 \mod 2\pi\mathbb{Z}\right\}$$

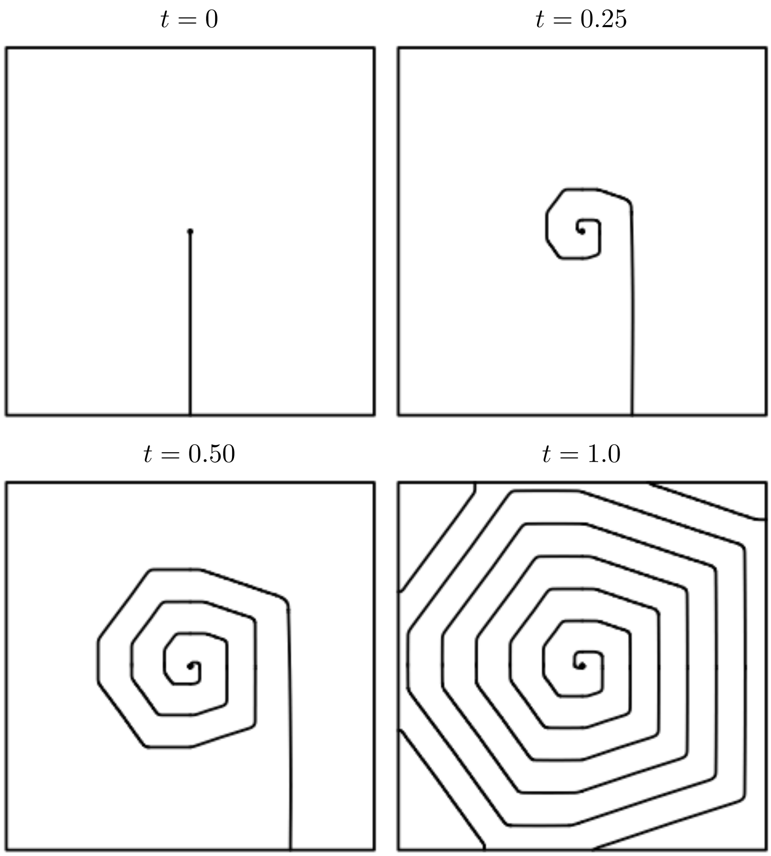

Figure 12. Profiles of a spiral at $t = 0, 0.25, 0.50$, and 1.0 evolving by (4.11) with Algorithm 1 and $\Delta x = 1/150$ ($s = 3$).

is divided by m_0 components of continuous curves $\Sigma_\ell(t)$ for $\ell = 0, 1, \dots, m_0 - 1$ as

$$\Sigma(t) = \bigcup_{\ell=0}^{m_0-1} \Sigma_\ell(t), \tag{4.12}$$

$$\Sigma_\ell(t) = \{x \in \overline{W} : u(t,x) - \theta(x) \equiv 2\pi\ell \mod 2\pi m_0\mathbb{Z}\}. \tag{4.13}$$

In such a case, we attempt to consider the situation such that each $\Sigma_\ell(t)$ evolves its own evolution equation

$$V_{\gamma_\ell} = f_\ell - \kappa_{\gamma_\ell} \quad \text{on } \Sigma_\ell(t) \tag{4.14}$$

by an anisotropic curvature κ_{γ_ℓ} with an anisotropic energy density γ_ℓ and a driving force f_ℓ

for $\ell = 0, 1, \dots, m_0 - 1$. We call such an evolution interlace motion. One can find such a situation in some real crystal growth experiments; see, for example, [40]. Its growth mechanism is understood as in [39].

We now give a formal discussion to examine the interlace motion with our algorithm. For simplicity of exposition, we tentatively assume that γ_ℓ are smooth so that the level set equation

$$\begin{aligned} &u_t + F_\ell(\nabla(u-\theta), \nabla^2(u-\theta)) = 0 \\ \text{where} \quad &F_\ell(\nabla w, \nabla^2 w) = \gamma_\ell(\nabla w)\{\operatorname{div}(\xi_\ell(\nabla w)) + f_\ell\}, \quad \xi_\ell = \nabla\gamma_\ell \end{aligned}$$

for (4.14) is well defined for each $\ell = 0, 1, \dots, m_0 - 1$. Due to the idea by [38], we now introduce a periodic cut-off function $\lambda : \mathbb{R}/(2\pi m_0 \mathbb{Z}) \to \mathbb{R}$; define

$$\lambda(\sigma) = \max\Big\{0, \min\Big\{1, \frac{\pi - |\sigma|}{\varepsilon} + \frac{1}{2}\Big\}\Big\}$$

for a constant $0 < \varepsilon \ll 1$. Note that λ satisfies

$$\begin{aligned} &\lambda(\sigma) = \begin{cases} 1 & \text{if } \sigma \in \Big[-\pi + \frac{\varepsilon}{2}, \pi - \frac{\varepsilon}{2}\Big], \\ 0 & \text{if } \sigma \in [-m_0\pi, m_0\pi] \setminus \Big(-\pi - \frac{\varepsilon}{2}, \pi + \frac{\varepsilon}{2}\Big), \end{cases} \\ &\sum_{\ell=0}^{m_0-1} \lambda(\sigma - 2\pi\ell) = 1. \end{aligned}$$

Then, formally, we find that the motion by (4.14) will be formulated with the solution $u(t, x)$ to

$$\begin{aligned} u_t &+ \lambda(u-\theta)F_0(\nabla(u-\theta), \nabla^2(u-\theta)) \\ &+ \lambda(u-\theta-2\pi)F_1(\nabla(u-\theta), \nabla^2(u-\theta)) \\ &+ \cdots + \lambda(u-\theta-2\pi(m_0-1))F_{m_0-1}(\nabla(u-\theta), \nabla^2(u-\theta)) = 0 \end{aligned} \tag{4.15}$$

in $(0, T) \times W$. Now, we consider the implicit difference scheme of (4.15) only in the time variable. Then, we obtain

$$\begin{aligned} u(t+h) &= u(t) \\ &+ h\sum_{\ell=0}^{m_0-1} \lambda(u(t+h)-\theta-2\pi\ell)F_\ell(\nabla(u(t+h)-\theta), \nabla^2(u(t+h)-\theta)). \end{aligned}$$

According to Section 2.2, the minimizer w_ℓ^* of

$$w \mapsto \int_W \gamma_\ell(\nabla(w-\theta))dx - \int_W f_\ell w dx + \frac{1}{2h}\Big\|\frac{w-u(t)}{\sqrt{\gamma_\ell(\nabla(u(t)-\theta))}}\Big\|_{L^2}^2$$

satisfies

$$\begin{aligned} w_\ell^* &= u(t) + h\gamma_\ell(\nabla(u(t)-\theta))\big\{\mathrm{div}\{\xi_\ell(\nabla(u(t+h)-\theta))\} + f_\ell\big\} \\ &\approx u(t) + hF_\ell(\nabla(u(t+h)-\theta), \nabla^2(u(t+h)-\theta)). \end{aligned}$$

Hence, we observe that

$$\begin{aligned} w^* &= \sum_{\ell=0}^{m_0-1} \lambda(u(t)-\theta-2\pi\ell)w_\ell^* \\ &\approx u(t) + h\sum_{\ell=0}^{m_0-1} \lambda(u(t)-\theta-2\pi\ell)F_\ell(\nabla(u(t+h)-\theta), \nabla^2(u(t+h)-\theta)) \end{aligned}$$

gives a finite difference scheme of (4.15). Thus, we define an algorithm of the interlace motion by (4.12), (4.13), and (4.14) as follows:

(1) For given Σ_n ($n \geq 0$) and $u_n \in C(\overline{W})$ satisfying

$$\begin{aligned} \Sigma_n &= \big\{x \in \overline{W} : u_n(x)-\theta(x) \equiv 0 \mod 2\pi\mathbb{Z}\big\}, \quad \mathbf{n} = -\frac{\nabla(u_n-\theta)}{|\nabla(u_n-\theta)|}, \\ \Sigma_{n,\ell} &= \big\{x \in \overline{W} : u_n(x)-\theta(x) \equiv 2\pi\ell \mod 2\pi m_0\mathbb{Z}\big\} \quad \text{for } \ell = 0,\dots,m_0-1, \end{aligned}$$

find the minimizer $w_\ell^* \in L^2(W) \cup BV(W)$ of

$$w \mapsto \int_W \gamma_\ell(\nabla(w-\theta))dx - \int_W f_\ell w dx + \frac{1}{2h}\left\| \frac{w-u_n}{\sqrt{\max\{\psi_\ell, \alpha\}}}\right\|_{L^2}^2$$

with $\psi_\ell = \gamma_\ell(\nabla(u_n-\theta))$ for every $\ell = 0,1,\dots,m_0-1$.

(2) Set

$$u_{n+1} = \sum_{\ell=0}^{m_0-1} \lambda(u_n-\theta-2\pi\ell)w_\ell^*$$

to return (1).

Figure 13 presents an example of interlace motion by two minor steps with a triangle anisotropy successively rotating π. The details of the setting are as follows:

$$\begin{cases} \text{Center}: N=1,\ a_1 = O,\ \theta(x) = 2\arg x, \\ \text{Evolution equation}: V_\ell = 3(1-0.02\kappa_\ell), \\ \text{Energy density}: \gamma_\ell(p) = \max\limits_{0\le j\le 2}(\cos\vartheta_{\ell,j}, \sin\vartheta_{\ell,j})\cdot p \\ \qquad \text{with } \vartheta_{\ell,j} = \dfrac{2\pi j}{3} + \dfrac{\pi}{6} + \pi\ell \quad (j=0,1,2,\ \ell=0,1), \\ \text{Initial data}: \text{The curve obtained from } u_0 = 0. \end{cases} \tag{4.16}$$

One can find a hexagonal pattern made by evolution and bunching of curves with triangle anisotropy.

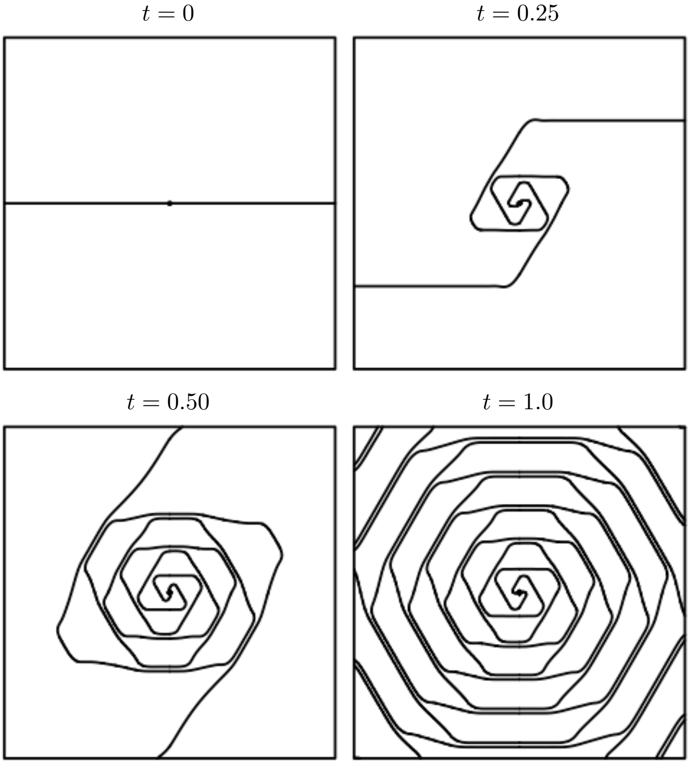

Figure 13. Profiles of interlace motion at $t = 0,\ 0.25,\ 0.5$, and 1.0 by (4.16).

Shtukenberg et al. [35] reports fascinating phenomena—so-called illusory loops and spirals. According to [35], L-cystine crystals have the following features:

- The crystal lattice has a hexagonal structure ($N_\gamma = 6$).
- The unit cell of the lattice consists of six layers ($m_0 = 6$) successively rotated clockwise by $\pi/3$.
- Each minor layer has a hexagonal pattern, whose unit cell has one facet having small energy density, and five facets having large energy density.

By the above structure, screw dislocation with the height of the unit molecule in an L-cystine crystal provides six minor steps evolving by hexagonal crystalline motion. Moreover, because of the asymmetry of energy density and the twisted structure of it, a bunch of minor steps forms

- a hexagonal target pattern (sequence of closed curves) even when the minor steps form spiral steps,

- a hexagonal spiral pattern even when the minor steps form closed curves.

We here propose a way to examine this situation using our approach.

By the above situation, we consider that the fundamental Wulff shape $\mathcal{W}_\gamma$ of minor steps satisfies the following:

- The unit normal vector $\mathbf{N}_j$ of j-th facet of $\mathcal{W}_\gamma$ is

$$\mathbf{N}_j = \left(\cos\frac{\pi j}{3}, \sin\frac{\pi j}{3}\right) \quad \text{for } 0 \le j \le 5. \tag{4.17}$$

- The surface energy of 0-th facet is a times of the other facets, that is,

$$\gamma(\mathbf{N}_0) = a\gamma(\mathbf{N}_j) \quad \text{for } 1 \le j \le 5, \tag{4.18}$$

  where $0 < a < 1$ is a constant.

Note that if the Frank diagram $\mathcal{F}_\gamma = \{p \in \mathbb{R}^2 : \gamma(p) \le 1\}$ is represented as a convex hull of its vertices $\mathbf{q}_j$, that is,

$$\mathcal{F}_\gamma = \left\{\sum_{j=0}^{N_\gamma - 1} c_j \mathbf{q}_j : 0 \le c_j \le 1, \sum_{j=0}^{N_\gamma - 1} c_j \le 1\right\},$$

then we observe that

$$\gamma^\circ(p) = \sup\{p \cdot q : \gamma(q) \le 1\} = \max_{0 \le j \le N_\gamma - 1} p \cdot \mathbf{q}_j.$$

Therefore, we now set the vertices $\mathbf{q}_j$ of $\mathcal{F}_\gamma$ as

$$\mathbf{q}_0 = \frac{1}{a}\mathbf{N}_0 = \left(\frac{1}{a}, 0\right), \quad \mathbf{q}_j = \mathbf{N}_j \quad \text{for } 1 \le j \le 5$$

to establish (4.17) and (4.18). To establish the successively rotating anisotropies of minor steps, we set

$$\gamma_\ell^\circ(p) = \max_{0 \le j \le 5} p \cdot \mathbf{q}_{j+\ell} \quad \text{for } 0 \le \ell \le 5. \tag{4.19}$$

Here, we have considered $j + \ell \in \mathbb{Z}/(6\mathbb{Z})$ in the above formula. See Figure 14 for the profiles of $\mathcal{W}_{\gamma_0}$ and $\mathcal{F}_{\gamma_0}$ for γ_0 and γ_0° using the above setting with $a = 0.5$.

Figure 15 and 16 show the profiles of illusory loops and spirals, respectively, by the above algorithm with $a = 0.5$. The settings are as follows:

- Evolution equation: $V_{\gamma_\ell} = 3(1 - 0.02\kappa_{\gamma_\ell})$ for $0 \le \ell \le 5$.
- Centers:
  - (Figure 15) $N = 1, a_1 = (0, 0), m_1 = 6$.
  - (Figure 16) $N = 2, a_1 = (-0.1, 0), a_2 = (0.1, 0), m_1 = 6, m_2 = -6$.
- Initial curve: Σ_0 is the curve given by setting $u_0 \equiv -\pi$.

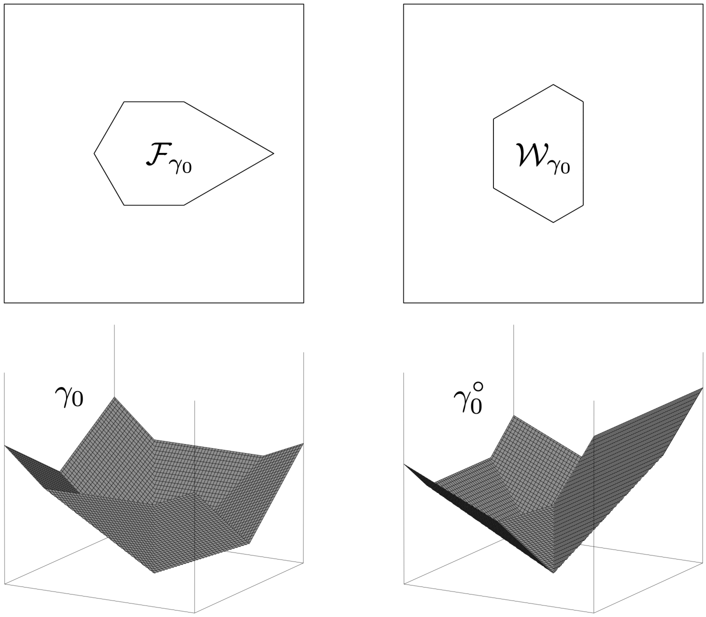

Figure 14. Graphs of γ_0 and $\mathcal{F}_{\gamma_0}$, or γ_0° and $\mathcal{W}_{\gamma_0}$ defined by (4.19) with $a = 0.5$.

In both cases, there are slower steps, catching the following faster steps, and then bunching phenomena make an irregular pattern against the situation of minor steps. In the case of Figure 15, each minor step forms a spiral curve that is not closed. However, bunches of minor steps make a target pattern that looks like a sequence of closed loops. Similarly, in the case of Figure 16, a bunch of minor steps make a spiral pattern, although each minor step forms a closed curve.

5. Summary

In this paper, we have introduced a minimizing movements algorithm based on [9, 26] for the evolution of spirals by crystalline curvature flow. Chambolle's formulation [9] involves a signed distance function to the interface. However, in the case of the evolving spirals, the signed distance function of a spiral curve is not convenient to work with, even in a small neighborhood around the spiral. Therefore, this paper introduced a modification that does not require the construction of signed distance functions after the time step. This modification, therefore, leads to a simpler numerical algorithm. As in the minimizing movements formulation, the algorithm requires solving optimization problems involving

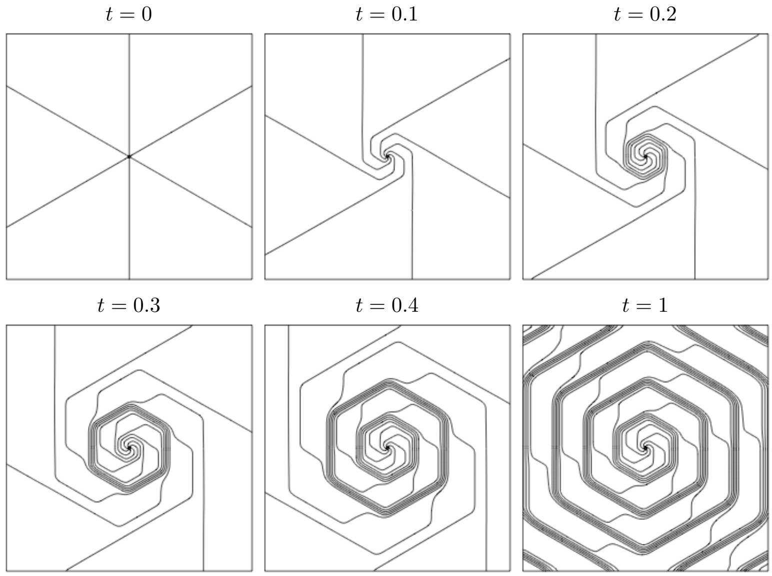

Figure 15. Numerical simulation forming illusory loops.

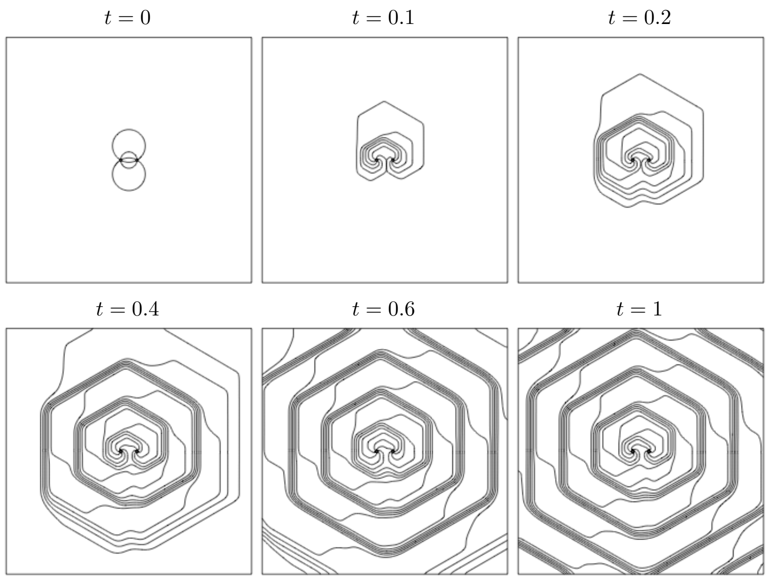

Figure 16. Numerical simulation forming illusory spirals.

L^1-type surface energy density. We proved the existence of minimizers for our approach (the functions whose zero level sets embed the spirals) and showed that the derivatives of the minimizers are in BV.

For the evolution of a single spiral, our computational results are very close to those computed by the front-tracking algorithm developed by [20]. Since our proposed algorithm for advancing the spiral involves outer and inner loops, we present empirical evidence that the number of inner and outer loops does not increase as the underlying Cartesian grid is refined.

By using level set functions, our approach enables us to handle merging of multiple spirals. Moreover, since our approach does not rely on the distance functions to the spirals, it allows us to handle the case in which bunching occurs. As applications of it, we showcased computational results on interlace motion [39,40], and illusory loops and spirals [35].

A. A front-tracking model for a single spiral

In this section we present a quick review of the model by [20].

Assume that $\mathcal{W}_\gamma$ is a convex polygon having N_γ facets. The normal and tangential vector of the j-th facet of $\mathcal{W}_\gamma$ is denoted by

$$\mathbf{N}_j = (\cos\widetilde{\vartheta}_j, \sin\widetilde{\vartheta}_j), \quad \mathbf{T}_j = (\sin\widetilde{\vartheta}_j, -\cos\widetilde{\vartheta}_j).$$

We also denote the length of the j-th facet as $\ell_j > 0$. We here assume that $\widetilde{\vartheta}_j$ satisfies (W1)–(W3), and extend ϑ_j from $j = 0, 1, \ldots, N_\gamma - 1$ to all $j \in \mathbb{Z}$ by

$$\widetilde{\vartheta}_{j+nN_\gamma} = \widetilde{\vartheta}_j + 2\pi n \quad \text{for } j = 0, 1, \ldots, N_\gamma - 1 \text{ and } n \in \mathbb{Z}.$$

We choose $\widetilde{\vartheta}_0 \in [-\pi, \pi)$ in this section. Accordingly, the facets of $\mathcal{W}_\gamma$ are numbered with counterclockwise rotation, and the numbering of facets are extended from $j = 0, 1, \ldots, N_\gamma - 1$ to $j \in \mathbb{Z}/(N_\gamma\mathbb{Z})$ as

$$\mathbf{N}_{j+nN_\gamma} = \mathbf{N}_j, \quad \mathbf{T}_{j+nN_\gamma} = \mathbf{T}_j, \quad \ell_{j+nN_\gamma} = \ell_j$$

for every $n \in \mathbb{Z}$ and $j = 0, 1, \ldots, N_\gamma - 1$. See Figure 17 for details of the notations for $\mathcal{W}_\gamma$.

Let $\Sigma_{\mathrm{d}}(t) = \bigcup_{j=0}^{k} \Sigma_{\mathrm{d},j}(t)$ be a polygonal spiral evolving by the front-tracking model of [20]. We denote the j-th facet of $\Sigma_{\mathrm{d}}(t)$ by $\Sigma_{\mathrm{d},j}(t)$. Here, we consider only the case when $\Sigma_{\mathrm{d}}(t)$ is convex, so that we assume that $\Sigma_{\mathrm{d},j}(t)$ is parallel to the j-th facet of $\mathcal{W}_\gamma$ for $j \in \mathbb{Z}/(N_\gamma\mathbb{Z})$. We also denote the center of $\Sigma_{\mathrm{d}}(t)$ by $y_k(t)$, and the vertices of $\Sigma_{\mathrm{d}}(t)$ by $y_{k-1}(t)$, $y_{k-2}(t), \ldots, y_1(t)$, and $y_0(t)$. Assume that $y_k(t) = O$, that is, the center is fixed at the origin. We also assume that $\Sigma_{\mathrm{d},0}(t)$ has infinite length. Then, $\Sigma_{\mathrm{d},j}(t)$ is

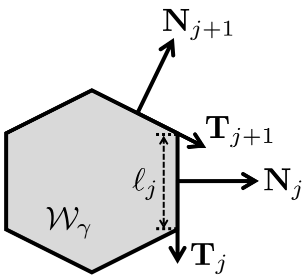

Figure 17. Notations for the Wulff diagram $\mathcal{W}_\gamma$.

described as

$$\Sigma_{\mathrm{d},j}(t) = \begin{cases} \{y_j(t) + \sigma \mathbf{T}_j : \sigma \in [0, d_j(t)]\} & \text{if } j = 1, 2, \ldots, k, \\ \{y_0(t) + \sigma \mathbf{T}_0 : \sigma \in [0, \infty)\} & \text{if } j = 0, \end{cases} \tag{A.1}$$

$$y_{j-1}(t) = y_j(t) + d_j(t)\mathbf{T}_j \quad \text{for } j = k, k-1, k-2, \ldots, 1, \tag{A.2}$$

$$y_k(t) = O, \tag{A.3}$$

where $d_j(t)$ denotes the length of $\Sigma_{\mathrm{d},j}(t)$. By the above formulation and [3,37], the crystalline curvature of $\Sigma_{\mathrm{d},j}(t)$ is defined by

$$\kappa_\gamma = \frac{\ell_j}{d_j(t)}.$$

Thus, (1.1) is translated as a formula of normal velocity V_j of j-th facet of the form

$$V_j = -\frac{\ell_j}{d_j} + f.$$

Consequently, the motion of $\Sigma_{\mathrm{d}}(t)$ by (1.1) is described by the evolution of $d_j(t)$ by the following ODE system:

$$\begin{cases} \dot{d}_k = c_k^-\Big(f - \dfrac{\ell_{k-1}}{d_{k-1}}\Big), \\ \dot{d}_{k-1} = -b_{k-1}\Big(f - \dfrac{\ell_{k-1}}{d_{k-1}}\Big) + c_{k-1}^-\Big(f - \dfrac{\ell_{k-2}}{d_{k-2}}\Big), \\ \dot{d}_j = -b_j\Big(f - \dfrac{\ell_j}{d_j}\Big) + c_j^+\Big(f - \dfrac{\ell_{j+1}}{d_{j+1}}\Big) + c_j^-\Big(f - \dfrac{\ell_{j-1}}{d_{j-1}}\Big) \\ \qquad\qquad\qquad\qquad\qquad\qquad \text{for } j = 2, 3, \ldots, k-2, \\ \dot{d}_1 = -b_1\Big(f - \dfrac{\ell_1}{d_1}\Big) + c_1^+\Big(f - \dfrac{\ell_2}{d_2}\Big) + c_1^- f, \end{cases} \tag{A.4}$$

where b_j and $c_j^\pm > 0$ are constants determined by $\widetilde{\vartheta}_j$. Moreover, the generation of a new facet at the origin is proposed in [20] for the evolution of a spiral; as the result of the motion of $\Sigma_{\mathrm{d}}(t)$, if the length of $\Sigma_{\mathrm{d},k}(t)$ reaches the critical length ℓ_k/f, then we add a new facet $\Sigma_{\mathrm{d},k+1}(\cdot)$ to Σ_{d} and change the fixed center of $\Sigma_{\mathrm{d}}(t)$ to $y_{k+1}(t)$ at $t = T_k$. In summary, an algorithm proposed in [20] is outlined as follows:

(1) Give an initial data $\Sigma_{\mathrm{d}}(0) = \bigcup_{j=0}^{k} \Sigma_{\mathrm{d},j}(0)$ with suitable initial data $d_j(0)$ for $j = 1, \dots, k-1$ and $d_k(0) = 0$. Set $T_{k-1} = 0$.

(2) Solve (A.4) in (T_{k-1}, ∞).

(3) Let us set $T_k = \sup\{T > T_{k-1} : d_k(t) < \ell_k/f \text{ for } t \in [T_{k-1}, T)\}$. If $T_k < \infty$, then we add a new facet $\Sigma_{\mathrm{d},k+1}(T_k)$ to $\Sigma_{\mathrm{d}}(T_k)$, and change the fixed center of $\Sigma_{\mathrm{d}}(t)$ to $y_{k+1}(t)$ at $t = T_k$.

(4) Return to (2), changing its center facet number k to $k+1$.

Note that the evolution law, in particular the behavior of the terminal facets $\Sigma_{\mathrm{d},k}(t)$ and $\Sigma_{\mathrm{d},0}(t)$ of the front-tracking model or the boundary condition are slightly different from our minimizing movements approach. However, in Section 4.1 we have seen that $\Sigma_{\mathrm{d}}(t)$ and $\Sigma_h(t)$ are numerically close.

B. Proof of Lemma 2.4

We now prove

(1) J_γ is convex and nonnegative.

(2) $J_\gamma(w) < \infty$ for $w \in BV(W)$.

(3) $\liminf_{u \to v} J_\gamma(u) \geq J_\gamma(v)$ in $L^1(W)$.

(4) If $w \in W^{1,1}(W)$, then $J_\gamma(w) = \int_W \gamma(\nabla(w - \theta))dx$.

However, we omit the proof of (1) since it is clear. See (2.11) for the definition of J_γ.

Proof. We demonstrate (2) and (3). Let $w \in BV(W)$ and $\varphi \in C_c^1(W; \mathbb{R}^2)$ with $\gamma^\circ(\varphi) \leq 1$. Note that

$$\begin{aligned} &\frac{1}{\Lambda_\gamma} \leq \gamma^\circ \leq \Lambda_\gamma \quad \text{on } \mathbb{S}^1, \\ &\gamma(p) \leq 1, \text{ or } \gamma^\circ(p) \leq 1 \quad \text{implies} \quad |p| \leq \Lambda_\gamma \end{aligned} \tag{B.1}$$

by (A2) and (A3). Then,

$$\begin{aligned} &-\int_W w \operatorname{div}\varphi dx - \int_W \nabla\theta \cdot \varphi dx \\ &\leq \|\varphi\|_\infty \Big(-\int_W w \operatorname{div} \frac{\varphi}{\|\varphi\|_\infty} dx \Big) + |W| \|\nabla\theta\|_\infty \|\varphi\|_\infty \\ &\leq \Lambda_\gamma([w]_{BV} + |W| \|\nabla\theta\|_\infty) \end{aligned}$$

by (B.1), where $|W|$ is a Lebesgue measure of W, and $\|\varphi\|_\infty = \sup_{\overline{W}} |\varphi|$. This implies (2).

Next, we observe that

$$\int_W u\mathrm{div}\varphi dx \to \int_W v\mathrm{div}\varphi dx \quad \text{as } u \to v \text{ in } L^1(W),$$

since $\mathrm{div}\varphi$ is bounded on $\overline{W}$. Hence, we obtain

$$\begin{aligned}\liminf_{u\to v} J_\gamma(u) &\geq \liminf_{u\to v}\Big[-\int_W u\mathrm{div}\varphi dx - \int_W \nabla\theta\cdot\varphi dx\Big]\\ &= -\int_W v\mathrm{div}\varphi dx - \int_W \nabla\theta\cdot\varphi dx,\end{aligned}$$

which implies (3).

Finally, we prove (4). First, let $w \in W^{1,1}(W)$ and $\varphi \in C_c^1(W;\mathbb{R}^2)$ with $\gamma^\circ(\varphi) \leq 1$. Then, we obtain

$$-\int_W w\mathrm{div}\varphi dx - \int_W \nabla\theta\cdot\varphi dx = \int_W \nabla(w-\theta)\cdot\varphi dx \leq \int_W \gamma(\nabla(w-\theta))dx,$$

since $\gamma(p) = \sup\{p\cdot q : \gamma^\circ(q) \leq 1\}$, which implies $J_\gamma(w) \leq \int_W \gamma(\nabla(w-\theta))dx$.

We next show that

$$\int_W \gamma(\nabla(w-\theta))dx \leq J_\gamma(w) \tag{B.2}$$

for $w \in W^{1,1}(W)$. We first note that γ is Lipschitz continuous, that is,

$$|\gamma(p_1)-\gamma(p_2)| \leq \Lambda_\gamma|p_1-p_2| \quad \text{for } p_1, p_2 \in \mathbb{R}^2. \tag{B.3}$$

This implies that

$$\Big|\int_W \gamma(\nabla(w-\theta))dx - \int_W \gamma(\nabla(v-\theta))dx\Big| \leq \Lambda_\gamma\|w-v\|_{W^{1,1}} \quad \text{for } w, v \in W^{1,1}(W).$$

Then, it suffices to prove (B.2) for $w \in C_c^1(\mathbb{R}^2)$, since $C_c^1(\mathbb{R}^2)$ is dense in $W^{1,1}(W)$.

We now make some preparations for the proof. Note that $\nabla(w-\theta)$ is uniformly continuous on $\overline{W}$. Let us fix $\varepsilon > 0$ as arbitrary, and fix $\delta > 0$ satisfying

$$\sup_{|y-x|<\delta} |\nabla(w-\theta)(y) - \nabla(w-\theta)(x)| < \frac{\varepsilon}{4\Lambda_\gamma|W|}.$$

Then, since $\{B_\delta(x) : x \in W\}$ is an open covering of $\overline{W}$, there exists $x_1, x_2, \dots, x_M \in W$ such that $\overline{W} \subset \bigcup_{j=1}^M B_\delta(x_j)$. Let $\chi_j : \mathbb{R}^2 \to [0, 1]$ be the partition of unity, that is, $\chi_j \in C^\infty(\mathbb{R}^2)$ for $j = 0, 1, \dots, M$ such that

- $\mathrm{supp}\chi_j \subset B_\delta(x_j)$ for $j = 1, \dots, M$, and $\mathrm{supp}\chi_0 \subset \mathbb{R}^2 \setminus \overline{W}$,
- $\sum_{j=0}^M \chi_j \equiv 1$, in particular $\sum_{j=1}^M \chi_j(x) = 1$ for $x \in \overline{W}$.

Let $q_{\varepsilon,j} \in \mathbb{R}^2$ be such that $\gamma^\circ(q_{\varepsilon,j}) \leq 1$ and

$$\gamma(\nabla(w-\theta)(x_j)) - \frac{\varepsilon}{2|W|} < \nabla(w-\theta)(x_j)\cdot q_{\varepsilon,j} \quad \text{for } j = 1,\dots,M.$$

Let $d(x)$ be a distance function of ∂W for $x \in \mathbb{R}^2$, that is,

$$d(x) = \begin{cases} \inf\{|x-y| : y \in \partial W\} & \text{if } x \in W, \\ -\inf\{|x-y| : y \in \partial W\} & \text{otherwise.} \end{cases}$$

Then, since ∂W is smooth, there exists $\delta_0 > 0$ such that $d \in C^1(\partial W^{\delta_0})$, where

$$\partial W^{\delta_0} = \left\{x \in \mathbb{R}^2 : |d(x)| < \delta_0\right\}.$$

We now consider a cut-off function $\zeta \in C^1(\mathbb{R})$ such that ζ is monotone nondecreasing and satisfies

$$\zeta(r) = \begin{cases} 0 & \text{if } r \leq 1/2, \\ 1 & \text{if } r \geq 1. \end{cases}$$

Then, we observe that $\widetilde{d}_n(x) = \zeta(nd(x)) \in C^1(\mathbb{R}^2)$ for sufficiently large $n \in \mathbb{N}$.

Set

$$\mathcal{J}(w;\varphi) = -\int_W w(y)\mathrm{div}\varphi(y)dy - \int_W \nabla\theta(y)\cdot\varphi(y)dy$$

for $w \in C_c^1(\overline{W})$ and $\varphi \in C_c^1(\overline{W};\mathbb{R}^2)$. We now choose $n \in \mathbb{N}$ sufficiently large so that $\widetilde{d}_n(x) \in C^1(\mathbb{R}^2)$, $\widetilde{d}_n(x_j) = 1$ for every $j = 1,\dots,M$, and

$$|\partial W^{\frac{1}{n}} \cap W| < \frac{\varepsilon}{\Lambda_\gamma(1+L)} \quad \text{where } L = \sup_{\overline{W}} |\nabla(w-\theta)|.$$

Note that

$$W \cap \partial W^{\frac{1}{n}} = \left\{x \in W : 0 \leq \widetilde{d}_n(x) < 1\right\}, \quad W \setminus \partial W^{\frac{1}{n}} = \{x \in W : \widetilde{d}_n(x) = 1\}.$$

Now, let us set $\varphi_\varepsilon(x) = \sum_{j=1}^M \widetilde{d}_n(x)\chi_j(x)q_{\varepsilon,j}$. Then, $\varphi_\varepsilon \in C_c^1(\overline{W};\mathbb{R}^2)$ and

$$\gamma^\circ(\varphi_\varepsilon(x)) \leq \sum_{j=1}^M \chi_j(x) = 1$$

for $x \in \overline{W}$ by (A1) and (A2). We now calculate $\mathcal{J}(w;\varphi_\varepsilon)$ with integration by parts and obtain

$$\begin{aligned} &\int_W \gamma(\nabla(w-\theta)(y))dy - \mathcal{J}(w;\varphi_\varepsilon) \\ &\quad = \int_W \big(\gamma(\nabla(w-\theta)(y)) - \nabla(w-\theta)(y)\cdot\varphi_\varepsilon(y)\big)dy = I + II, \end{aligned} \tag{B.4}$$

where

$$I = \int_{W_1} \big(\gamma(\nabla(w-\theta)(y)) - \nabla(w-\theta)(y)\cdot\varphi_\varepsilon(y)\big)dy, \quad W_1 = W \setminus \partial W^{\frac{1}{n}},$$
$$II = \int_{W_2} \big(\gamma(\nabla(w-\theta)(y)) - \nabla(w-\theta)(y)\cdot\varphi_\varepsilon(y)\big)dy, \quad W_2 = W \cap \partial W^{\frac{1}{n}}.$$

In the first part, since $\widetilde{d}_n = 1$ on W_1, we have

$$I = \sum_{j=1}^{M} \int_{W_1\cap B_\delta(x_j)} \chi_j(y)\big(\gamma(\nabla(w-\theta)(y)) - \nabla(w-\theta)(y)\cdot q_{\varepsilon,j}\big)dy.$$

For $y \in W_1 \cap B_\delta(x_j)$, we observe that

$$\begin{aligned}
&\gamma(\nabla(w-\theta)(y)) - \nabla(w-\theta)(y)\cdot q_{\varepsilon,j}\\
&\quad\le \gamma(\nabla(w-\theta)(x_j)) - \nabla(w-\theta)(x_j)\cdot q_{\varepsilon,j}\\
&\qquad + (\Lambda_\gamma + |q_{\varepsilon,j}|)|\nabla(w-\theta)(y) - \nabla(w-\theta)(x_j)|\\
&\quad< \frac{\varepsilon}{|W|}
\end{aligned}$$

by (B.3) and (B.1). Then, we obtain

$$I < \frac{\varepsilon}{|W|}\sum_{j=1}^{M}\int_{W_1\cap B_\delta(x_j)} \chi_j(y)dy = \varepsilon. \tag{B.5}$$

On the second part of (B.4), we give an estimate of

$$II = \sum_{j=1}^{M} \int_{W_2\cap B_\delta(x_j)} \chi_j(y)\big(\gamma(\nabla(w-\theta)(y)) - \widetilde{d}_n(y)\nabla(w-\theta)(y)\cdot q_{\varepsilon,j}\big)dy.$$

Note that $\gamma(p) \le \Lambda_\gamma|p|$ for every $p \in \mathbb{R}^2$. Thus, we have

$$\begin{aligned}
&\big|\gamma(\nabla(w-\theta)(y)) - \widetilde{d}_n(y)\nabla(w-\theta)(y)\cdot q_{\varepsilon,j}\big|\\
&\quad\le \gamma(\nabla(w-\theta)(y)) + |\nabla(w-\theta)(y)||q_{\varepsilon,j}|\\
&\quad\le 2\Lambda_\gamma L
\end{aligned}$$

for $y \in W_2 \cap B_\delta(x_j)$. Hence, we obtain

$$|II| \le 2\Lambda_\gamma L \sum_{j=1}^{M}\int_{W_2\cap B_\delta(x_j)} \chi_j(y)dy = 2\Lambda_\gamma L|W_2| \le 2\varepsilon. \tag{B.6}$$

By combining (B.4), (B.5), and (B.6), we obtain

$$\int_W \gamma(\nabla(w-\theta)(y))dy - \mathcal{J}(w;\varphi_\varepsilon) \le 3\varepsilon,$$

which implies

$$\int_W \gamma(\nabla(w-\theta))dx \le J_\gamma(w) + 3\varepsilon.$$

Letting $\varepsilon \to 0$, we obtain (B.2) for $w \in C_c^1(\mathbb{R}^2)$, and thus (4). ∎

Acknowledgements. The authors are grateful to Professor Y. Giga for valuable comments and for bringing the papers [14, 17, 27] to their attention. The authors are also grateful to anonymous referees for valuable suggestions to improve the presentation of this paper.

Funding. The work of Ohtsuka is partly supported by JSPS KAKENHI Grant Number 21K03319. Tsai is partially supported by NSF Grant DMS-2110895. Tsai also acknowledges support from the National Center for Theoretical Sciences (NCTS), Taiwan, during his visits.

References

[1] F. Almgren and J. E. Taylor, Flat flow is motion by crystalline curvature for curves with crystalline energies. *J. Differential Geom.* **42** (1995), no. 1, 1–22 Zbl 0867.58020 MR 1350693

[2] F. Almgren, J. E. Taylor, and L. Wang, Curvature-driven flows: a variational approach. *SIAM J. Control Optim.* **31** (1993), no. 2, 387–438 Zbl 0783.35002 MR 1205983

[3] S. Angenent and M. E. Gurtin, Multiphase thermomechanics with interfacial structure. II. Evolution of an isothermal interface. *Arch. Rational Mech. Anal.* **108** (1989), no. 4, 323–391 Zbl 0723.73017 MR 1013461

[4] G. Barles and C. Georgelin, A simple proof of convergence for an approximation scheme for computing motions by mean curvature. *SIAM J. Numer. Anal.* **32** (1995), no. 2, 484–500 Zbl 0831.65138 MR 1324298

[5] G. Barles, H. M. Soner, and P. E. Souganidis, Front propagation and phase field theory. *SIAM J. Control Optim.* **31** (1993), no. 2, 439–469 Zbl 0785.35049 MR 1205984

[6] G. Bellettini and M. Paolini, Anisotropic motion by mean curvature in the context of Finsler geometry. *Hokkaido Math. J.* **25** (1996), no. 3, 537–566 Zbl 0873.53011 MR 1416006

[7] L. M. Brègman, A relaxation method of finding a common point of convex sets and its application to the solution of problems in convex programming. *Ž. Vyčisl. Mat i Mat. Fiz.* **7** (1967), 620–631 Zbl 0186.23807 MR 215617

[8] W. K. Burton, N. Cabrera, and F. C. Frank, The growth of crystals and the equilibrium structure of their surfaces. *Philos. Trans. Roy. Soc. London Ser. A* **243** (1951), 299–358 Zbl 0043.23402 MR 43005

[9] A. Chambolle, An algorithm for mean curvature motion. *Interfaces Free Bound.* **6** (2004), no. 2, 195–218 Zbl 1061.35147 MR 2079603

[10] X. Chen, Generation and propagation of interfaces for reaction-diffusion equations. *J. Differential Equations* **96** (1992), no. 1, 116–141 Zbl 0765.35024 MR 1153311

[11] L. C. Evans and R. F. Gariepy, *Measure theory and fine properties of functions*. Studies in Advanced Mathematics, CRC Press, Boca Raton, FL, 1992 Zbl 0804.28001 MR 1158660

[12] L. C. Evans, H. M. Soner, and P. E. Souganidis, Phase transitions and generalized motion by mean curvature. *Comm. Pure Appl. Math.* **45** (1992), no. 9, 1097–1123 Zbl 0801.35045 MR 1177477

[13] L. C. Evans and J. Spruck, Motion of level sets by mean curvature. I. *J. Differential Geom.* **33** (1991), no. 3, 635–681 Zbl 0726.53029 MR 1100206

[14] M.-H. Giga, Y. Giga, and H. Hontani, Self-similar expanding solutions in a sector for a crystalline flow. *SIAM J. Math. Anal.* **37** (2005), no. 4, 1207–1226 Zbl 1093.74048 MR 2192293

[15] M.-H. Giga, Y. Giga, R. Kuroda, and Y. Ochiai, Crystalline flow starting from a general polygon. *Discrete Contin. Dyn. Syst.* **42** (2022), no. 4, 2027–2051 Zbl 1494.53108 MR 4385786

[16] Y. Giga, *Surface evolution equations*. Monogr. Math. 99, Birkhäuser, Basel, 2006 Zbl 1096.53039 MR 2238463

[17] Y. Giga and N. Požár, Motion by crystalline-like mean curvature: a survey. *Bull. Math. Sci.* **12** (2022), no. 2, article no. 2230004 Zbl 1504.35002 MR 4460400

[18] T. Goldstein and S. Osher, The split Bregman method for $L1$-regularized problems. *SIAM J. Imaging Sci.* **2** (2009), no. 2, 323–343 Zbl 1177.65088 MR 2496060

[19] T. Ishiwata, Crystalline motion of spiral-shaped polygonal curves with a tip motion. *Discrete Contin. Dyn. Syst. Ser. S* **7** (2014), no. 1, 53–62 Zbl 1273.82076 MR 3082855

[20] T. Ishiwata and T. Ohtsuka, Evolution of a spiral-shaped polygonal curve by the crystalline curvature flow with a pinned tip. *Discrete Contin. Dyn. Syst. Ser. B* **24** (2019), no. 10, 5261–5295 Zbl 1423.34023 MR 4026926

[21] T. Ishiwata and T. Ohtsuka, Numerical analysis of an ODE and a level set methods for evolving spirals by crystalline Eikonal-curvature flow. *Discrete Contin. Dyn. Syst. Ser. S* **14** (2021), no. 3, 893–907 Zbl 1467.65068 MR 4219086

[22] R. Kobayashi, A brief introduction to phase field method. *AIP Conf. Proc.* **1270** (2010), 282–291

[23] S. Luckhaus and T. Sturzenhecker, Implicit time discretization for the mean curvature flow equation. *Calc. Var. Partial Differential Equations* **3** (1995), no. 2, 253–271 Zbl 0821.35003 MR 1386964

[24] B. Merriman, J. Bence, and S. Osher, Diffusion generated motion by mean curvature. In *Computational Crystal Growers Workshop*, edited by J. E. Taylor, pp. 73–83, Sel. Lectures Math., American Mathematical Society, Providence, RI, 1992

[25] H. Miura and R. Kobayashi, Phase-field modeling of step dynamics on growing crystal surface: Direct integration of growth units to step front. *Cryst. Growth Des.* **15** (2015), no. 5, 2165–2175

[26] A. Oberman, S. Osher, R. Takei, and R. Tsai, Numerical methods for anisotropic mean curvature flow based on a discrete time variational formulation. *Commun. Math. Sci.* **9** (2011), no. 3, 637–662 Zbl 1273.35027 MR 2865799

[27] Y. Ochiai, *Facet-creation between two facets movend by crystalline curvature*. Master's Thesis, The University of Tokyo, 2009

[28] T. Ohtsuka, A level set method for spiral crystal growth. *Adv. Math. Sci. Appl.* **13** (2003), no. 1, 225–248 Zbl 1059.74045 MR 2002402

[29] T. Ohtsuka, Minimizing movement approach for spirals evolving by crystalline curvature using level set functions. *Oberwolfach Reports* **14** (2017), 314–317

[30] T. Ohtsuka, Minimizing movement approach without using distance function for evolving spirals by the crystalline curvature with driving force. *RIMS Kôkyûroku* **2121** (2019), 74–87

[31] T. Ohtsuka, Y.-H. R. Tsai, and Y. Giga, A level set approach reflecting sheet structure with single auxiliary function for evolving spirals on crystal surfaces. *J. Sci. Comput.* **62** (2015), no. 3, 831–874 Zbl 1331.53101 MR 3304334

[32] T. Ohtsuka, Y.-H. R. Tsai, and Y. Giga, Growth rate of crystal surfaces with several dislocation centers. *Crystal Growth & Design* **18** (2018), no. 3, 1917–1929

[33] S. Osher, M. Burger, D. Goldfarb, J. Xu, and W. Yin, An iterative regularization method for total variation-based image restoration. *Multiscale Model. Simul.* **4** (2005), no. 2, 460–489 Zbl 1090.94003 MR 2162864

[34] R. T. Rockafellar, *Convex analysis*. Princeton Landmarks Math., Princeton University Press, Princeton, NJ, 1997 Zbl 0932.90001 MR 1451876

[35] A. G. Shtukenberg, Z. Zhu, Z. An, M. Bhandari, P. Song, B. Kahr, and M. D. Ward, Illusory spirals and loops in crystal growth. *Proc. Natl. Acad. Sci. USA* **110** (2013), no. 43, 17195–17198

[36] H. M. Soner, Motion of a set by the curvature of its boundary. *J. Differential Equations* **101** (1993), no. 2, 313–372 Zbl 0769.35070 MR 1204331

[37] J. E. Taylor, Constructions and conjectures in crystalline nondifferential geometry. In *Differential geometry*, pp. 321–336, Pitman Monogr. Surveys Pure Appl. Math. 52, Longman Sci. Tech., Harlow, 1991 Zbl 0725.53011 MR 1173051

[38] Y.-H. Tsai and Y. Giga, A numerical study of anisotropic crystal growth with bunching under very singular vertical diffusion. *Hokkaido University Preprint Series in Mathematics* 591 (2003), 1–9.

[39] W. J. P. van Enckevort and P. Bennema, Interlacing of growth steps on crystal surfaces as a consequence of crystallographic symmetry. *Acta Crystallographica Section A* **60** (2004), no. 6, 532–541

[40] A. R. Verma, CI. Observations on carborundum of growth spirals originating from screw dislocations. *The London, Edinburgh, and Dublin Philosophical Magazine and Journal of Science* **42** (1951), no. 332, 1005–1013

[41] S. Yazaki, Point-extinction and geometric expansion of solutions to a crystalline motion. *Hokkaido Math. J.* **30** (2001), no. 2, 327–357 Zbl 1192.82077 MR 1844823

Received 24 September 2024; revised 4 April 2025.

Takeshi Ohtsuka
Faculty of Informatics, Gunma University, 4-2 Aramakicho, Maebashi, Gunma 371-8510, Japan; tohtsuka@gunma-u.ac.jp

Yen-Hsi Richard Tsai
Department of Mathematics and Oden Institute for Computational Engineering and Sciences, The University of Texas at Austin, 201 E. 24th Street, POB 4.102, Austin, TX 78712, USA; ytsai@math.utexas.edu